Modeling crop growth using multisensor analysis in remote sensing

Auteur : Bataille, Laurent
Promoteur(s) : Meersmans, Jeroen; Heidarian Dehkordi, Ramin
Faculté : Gembloux Agro-Bio Tech (GxABT)
Diplôme : Master en bioingénieur : sciences et technologies de l'environnement, à finalité spécialisée
Année académique : 2020-2021
URI/URL : http://hdl.handle.net/2268.2/13176

LIÈGE université
Gembloux
Agro-Bio Tech

Modeling crop growth using multisensor analysis in remote sensing

Laurent Bataille

TRAVAIL DE FIN D'ETUDES PRÉSENTÉ EN VUE DE L'OBTENTION DU DIPLÔME DE MASTER BIOINGÉNIEUR EN SCIENCES ET TECHNOLOGIES DE L'ENVIRONNEMENT

ANNÉE ACADEMIQUE 2020 - 2021

Co-promoteurs:
Pr. Jeroen Meersmans
Pr. Joost Wellens
PhD Ramin Heidarian Dehkordi
Pr. Jean-François Bastin

[1] L'autorité académique est représentée par le promoteur, membre du personnel enseignant de GxABT (Jeroen Meersmans - jeroen.meersmans@uliege.be)

[2] The academic authority is represented by the thesis supervisor, a member of the GxABT teaching staff (Jeroen Meersmans) jeroen.meersmans@uliege.be

LIÈGE université
Gembloux
Agro-Bio Tech

Modeling crop growth using multisensor analysis in remote sensing

Laurent Bataille

TRAVAIL DE FIN D'ETUDES PRÉSENTÉ EN VUE DE L'OBTENTION DU DIPLÔME DE MASTER BIOINGÉNIEUR EN SCIENCES ET TECHNOLOGIES DE L'ENVIRONNEMENT

ANNÉE ACADEMIQUE 2020 - 2021

Co-promoteurs:
Pr. Jeroen Meersmans
Pr. Joost Wellens
PhD Ramin Heidarian Dehkordi
Pr. Jean-François Bastin

Acknowledgement/Remerciements

Avec ce TFE, c'est un très long chapitre de ma vie qui va se refermer. Ces remerciements manqueront de concision, ceci n'est pas un spoiler, pour celles et ceux qui me connaissent un peu. Le voyage fut long, la destination finale changeant sans cesse, m'apprenant des choses tout autant sur le monde et que sur soi-même. Mais ceci signifie que j'ai rencontré quantité de gens formidables et inoubliables en chemin.

Merci à ma mère de m'avoir soutenu pendant toutes ces années.

Merci à ces nombreux professeurs inspirants qui ont jalonné mon aventure académiques, auxquels je ne pourrai jamais rendre ce qu'il m'ont apporté. Christian Guillaume, Catherine Van Damme, Michel Hubin de l'Athénée Royal de Saint-Georges sur Meuse, Silvia Blacher, Rodolphe Sepulchre, Pierre Dauby, Nicolas Vandewalle, Quentin Louveaux et Christophe Geuzaine de l'ULiège, Bernard Heinesch, Aurore Degré, Gilles Colinet et Vincent Leemans de Gembloux Agro BioTech.

Merci à mes encadrants pour ce TFE, Jeroen Meersmans, Joost Wellens, Ramin Heidarian Dehkordi pour leur soutien sans faille, leur disponibilité, leurs conseils, leur bienveillance et leur expertise que je n'ai probablement pas apprécier à leur juste valeur, je ne pouvais rêver mieux. Je les remercie particulièrement d'avoir canalisé ma curiosité et d'avoir fait preuve d'une patience extrême quant à ma propension parfois encombrante à dériver un peu vers des objectifs secondaires.

My heartfelt thanks to all my supervisors for this master thesis, Jeroen Meersmans, Joost Wellens, Ramin Heidarian Dehkordi. I could not ask for a better committee, I thank you for your support, your availability, your great advices and your expertise. I thank them a lot

to funnel my curiosity and your patience toward obsession with details and my tendency to focus secondary objectives.

Merci à Marie Weiss, Benjamin Dumont et Jurgen Everaerts d'avoir pris le temps de répondre à mes questions par e-mail, de m'avoir redirigé vers la documentation appropriée.

Merci à Catherine Charles, Aurore Degré et Gilles Colinet pour leur soutien, ils ont eu un rôle discret mais déterminant dans ce tfe.

Merci à Laurent, Charles, Neville, Delphine, Nicolas, Fadoua, David, Pierre, Mike, Corentin et tant d'autres rencontrés à l'ULg puis perdus de vue au fil du temps.

Merci aux amis de l'INeE, particulièrement Grégory, Cécile, Isabelle, Claire, Sébastien, Gabriel L., Amir, Yvan et Gilles.

Merci à la très grande famille gembloutoise de m'avoir accueilli, j'ai eu le privilège de fréquenter énormément de groupes lors de ma première année ici. Merci à celles et ceux qui m'ont soutenu dans les moments plus compliqués, particulièrement. Noé, Martin, Keb le Sage, Sophie, Nicolas M., Lisa, Anna, Sasha, Yorick, Nina, Sarah, Florine J., Laurie, Arnaud M., Adèle, Claire M, Grégoire, Florine P., Vyckie Vyckie, Manu, Simon M., Maxence , Lallie, Sébastien, Arnaud B., Benoît, Zineb, Coralie, Marie, Sandy, Loïc, Sibylle, Marie K., Aurélien, Gaspard C., Lucien, Louise, Alexandre P., Cyril, Guillaume C., Lolita, Orion, Student, Killian R., Marco, Eddy, Rack, Quintal, Pils, Roxane, Rudie, Floppine, Alexis, Ruche, Alexandre D., Corentin, Roxane, Violette, Lucie V., Samuel, Claire S., Olivier, Florence, Mathilde, Séverine C., Lucie R., Lucie J., Killian D., , Tom L., Harold t'S, Florian M., Diego, Tom M., Anouk, Guillaume N., Séverine D., Noémie, Samy, Gaspard E., Thibault, Mattia, Ignace, Nathan, Baptise, Quentin, Zoë, Alice, Hélène, Thomas D., Soleiman, Laura, Thomas P., Cédric L., Damien, Edouard, Lucas M., Maxime L., Jeanine, Bernard, Jérôme, Cédric M., Vincent V., Gauthier, Pierre-Edouard, Andyne, Black-T, Rasti, Anthony ElFlamouchos, Jérémie, Calvi, Germouille, Bourlon, Johny & Nickie,

Merci à Matthieu, Nico, Noémie, Victor, Marie, Noé et Adèle pour l'ambiance chaleureuse du TOPO.

Merci l'office, aux Off-sets, aux Abbayistes, aux kots de l'auberge, de la grange, au KC, au Blokker, à la chiée des glands, au Déchets, au Liroux, au Gucci, aux amis de l'AG... Merci à tous les amis de la commission Impro, de Ventana et à toute l'équipe du VagaFestoch' (dédicace à l'équipe Psyterie), à tous les participants à la formation GBXLaTeX. Merci à la comission Eric & Dominique.

Je poume tous les altruistes désintéressés qui parviennent toujours à libérer du temps pour les autres et ceux qui n'ont jamais n'hésité pas à partager le fruit de leur travail avec le plus grand nombre, qu'il s'agisse de synthèses, de tuyaux ou de codes.

Résumé

Ces dernières années, l'utilisation d'images satellitaires et drones a connu un développement exponentiel dans le domaine agronomiquee . Ces deux approches semblent très complémentaires en termes de couverture temporelle et de résolution spatiale. L'objectif principal de ce travail est de confronter les deux à l'échelle d'une parcelle de froment d'hiver au fil d'une saison de culture via des séries temporelles de la fraction de couvert vert (FCOVER) et de les combiner pour caractériser mieux de la croissance de la culture. Les images multibandes sont couplées à des images Sentinel2 sur la même période. L'objectif secondaire consiste en l'exploitation les outils implémentés pour déterminer l'influence d'éléments micropaysagers de la parcelle sur la croissance de la culture. Les premiers résultats de cette étude sont purement méthodologiques. Comparer efficacement ces séries temporelles a nécessité la mise en place d'un algorithme permettant de condenser l'information dans les paramètres d'un modèle de croissance et d'exploiter finalement ce molèle pour simuler le rendement via d'Aquacrop OS. L'ensemble de ces paramètres sont synthétisés sous forme de cartes. Une carte de rendement au moyen d'un modèle empirique a permis de confronter les performances des différentes approches. Les données Sentinel2 (resp. drone) débouchent sur une sous-estimation (resp. sur-estimation) du rendement à l'hectare, tandis que les méthodes combinant les données tendent vers une estimation plus proche de la carte de référence. En outre, une comparaison entre les résultats développés ci-dessus et un ensemble de covariables liées à la topographie, à la date de labour et à la présence d'aire de faulde ont mis en évidence une croissance plus rapide et des rendements plus élevés sur le versant orienté au sud, tendance accrue par un labour précoce et les aires de faulde.

Mots clés : Froment d'hiver, modèle de croissance, Aquacrop, SNAP, FCOVER, FVC, télédétection, drone, Belgique, rendements à l'hectare, aire de faulde

Abstract

These last years, the use of spaceborne remote sensing and unmanned aerial vehicles (UAV) has grown exponentially in agronomy. Their abilities are theoretically complementary in terms of temporal coverage and spatial resolution. This work aims to compare both approaches at the scale of a winter wheat experimental parcel during a complete growing season using green fractional cover time-series (FCOVER) and combine them to improve crop growth characterization. UAV multibands images and Sentinel2 images are analyzed on the same time interval. Eventually, the influence of landscape elements on crop growth-related variables is studied. The methodological results of this study are the processes used to transpose FCOVER time-series into a reduced amount of crop growth parameters and quantify their uncertainties. These parameters allow predicting yield using the Aquacrop Model and finally summarizing this information on a set of maps. A comparison between yield predictions to a reference yield map based on field measurement shows that yield prediction using S2 (resp.UAV) FCOVER tends to underestimate (resp. overestimate), while data combination tends to be closer to reference values.UAV provides earlier and faster growth curves, reaching higher maxima. Growth process variables are compared to covariables describing topography, the presence of historical charcoal kilns, and the ploughing date. South facing half of the parcel experiences faster growth and higher yield; an earlier ploughing date and biochar patches emphasize this trend.

Keywords : Winter wheat, crop growth, Aquacrop, SNAP, remote sensing, unmanned aerial vehicle, FCOVER , FVC, Belgium, Yield, historical kilns

Contents

List of Figures

List of Tables

Contextualisation

For decades, the acquisition and the processing of images of the Earth's surface have become priorities of multiple space agencies. These last years, the advent of an open access policy, materialized by publicly funded space programs such MODIS, LANDSAT, MERIS and more recently Copernicus, has dramatically creased the use of remote sensing data in environmental sciences and agronomy.

Remote sensing allows study areas at a considerable scale at a reduced cost for agronomists; it has become one of the primary data supplies used by a new trend in agronomy, while data sciences expand concomitantly in agronomy giving rise to Smart Farming. More recently, UAV data collection tools have also opened to civil society providing datasets whose spatial accuracy at a local scale surpass what already existed in remote sensing.

Usually, both approaches provide results whose potentialities are pretty complementary; satellite data are provided regularly at coarse resolution, while UAV data resolution is very high but available less frequently and requires the presence of a human operator. As a result, crop growth monitoring tools focus on satellite datasets processing. However, UAV-resolution datasets require more storage resources, and processing them is more computationally expensive for equivalent area coverage. Consequently, algorithms used to extract the same features varies depending on the used resolutions. UAV high resolution allows quickly implementing semi-empirical models from field data, such as predicting the yields, developing crop health/development indicators, or decision support systems dedicated to irrigation and fertilization. Data fusion processes between satellite images of different resolutions are studied for years. However, the scale disparity between UAV and satellite images is so high that it requires innovative methods to practice data fusion and existing algorithms to serve a specific scientific purpose.

This work aims to compare both kinds of processing at the scale of a winter wheat experimental parcel during a complete growing season using green fractional cover time-series (FCOVER) and attempts to combine both datasets with improving crop growth characterization. FCOVER is one of the easiest proxies of the green biomass to measure using remote sensing. In 2019 UAV images were collected by (Heidarian Dehkordi et al. 2020) in order to compare crop growth on century old biochar spots and the adjacent soils. This parcel lies on loamy soil in Isnes, Belgium. This study compares these high resolution UAV images to Sentinel2 images with a 10m resolution.

Aquacrop is an open-source freeware developed by FAO. This software is dedicated to the decision support system, simulating variables of interest such as daily evapotranspiration and yield according to different scenarios. The model's inputs are climate datasets, soil hydrological properties, and crop characteristics, including a growth model based on an FCOVER parametrization. Simulations are performed at the scale of the studied parcel to predict yield maps from the FCOVER time series.

The results of the different models are compared to various parcel covariates to determine their influence on growth process variables and yield. Most of the covariates are related to topography except ploughing date and the presence of century-old biochar patches.

Chapter 1

State of the Art

1.1 Crop of interest - Winter Wheat

In 2019, wheat was grown on 215 million hectares, a surface equivalent to Greenland distributed worldwide (FAOSTAT 2019). This same year, the world wheat production reached 747 million metric tons (USDA 2021) while being the second most consumed directly by man after rice. The nutritional value of Wheat Grain is very high; wheat contains fibers, vitamins, amino acids, and minerals (Sramkova, Gregová, and Šturdík 2009).

Moreover, its domestication induced the emergence and development of agriculture in middle-east during the neolithic (Venske et al. 2019). As a result, this cereal is the most studied in the history of humanity; centuries of genetic selection created countless regional strains with different yields and abilities to resist environmental stress such as diseases, extreme temperature, and precipitation (Cossani and Reynolds 2012).

Phenology : Growth Cycle

Winter Wheat (Triticum aestivum L.) is a strain of wheat that is sowed in Belgium from autumn to the beginning of winter and harvested during the following summer. The growth rate depends mainly on temperature and photoperiod in optimal growing conditions without biotic or water stress. Dependence on photoperiod disappears after wheat flowering (Brisson et al. 2010). Figure 1.1 shows the complete growth cycle of winter wheat.

The emergence stage starts when the first leaf crosses the rigid and protective sheath that surrounds the coleoptile. The duration of this stage is the time between the sowing date and the emergence date. Different steps occur during this stage: germination, elongation of the first leaf's coleoptile, and growth. A molecular regulation prevents a direct transition to

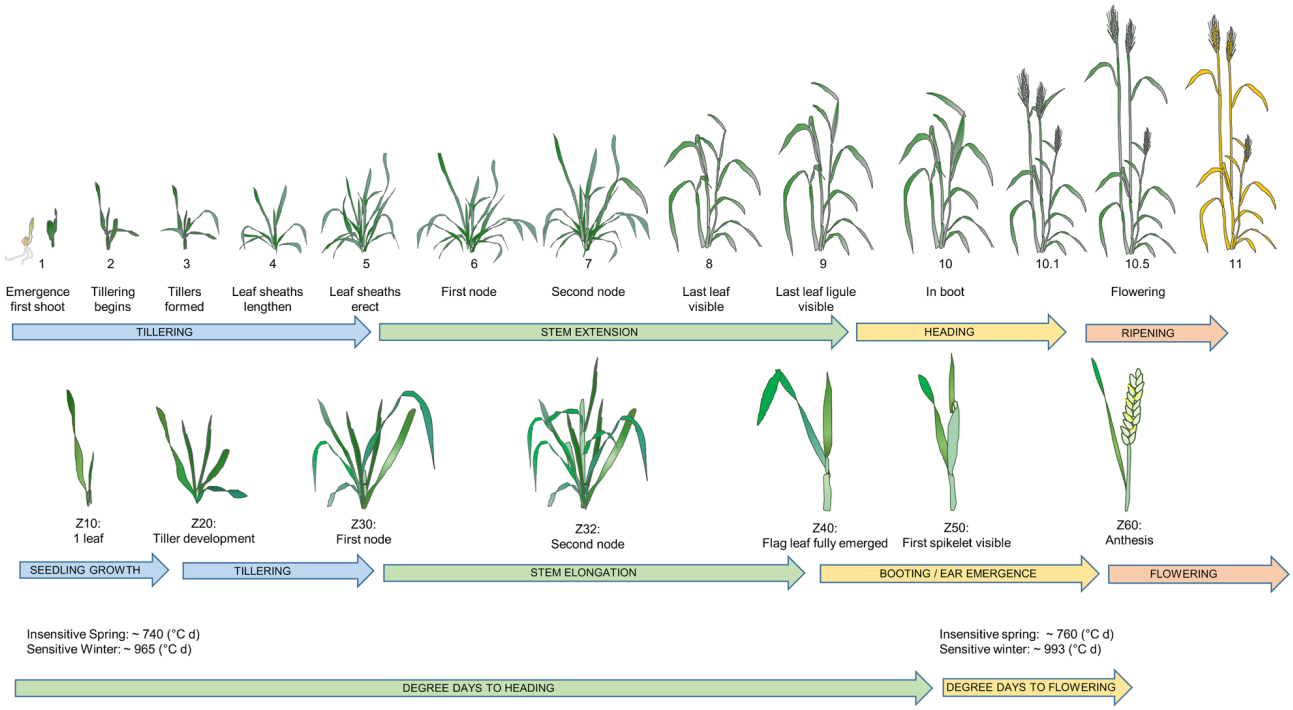

Figure 1.1: Winter Wheat Development - (Hyles et al. 2020)

reproductive development before exposure to the prolonged cold of winter (G. Li et al. 2013). This mechanism is called vernalization. Young plants are very resistant to frost, while frost resistance progressively decreases during heading and flowering. Vernalization can last 30 to 60 days of cold winter temperature, wheat growth restart, and complete emergence. The next step is tillering; grassland produces a stem, which is followed by tillering. On average, a temperature sum of 550 to 650 degrees day (base 0°C) is required after sowing to reach this stage (Gate 1995).

The plant counts three or four leaves; tillering occurs at the emergence of a new stem (called a tiller). When tillering stage ends, the plants straighten, and the first node appears on the tillers. Simultaneously, first leaf sheaths lengthen (Gate 1995). Terminal spikelets starts developing.

It marks the beginning of stem elongation. The stem consists of stacked nodes; internodes are the length of the stem between nodes. The growth of the first internodes is the first step of stem elongation begins, and internodes elongate in their order of successive appearance. Leaf-sheaths are now strongly erected.

At the end of stem elongation, the sheath of the last leaf is spreading and the top of the ear is coming out (Wise et al. 2011). Then, the booting phase starts, the stems keep elongating, spikelets become more and more visible. Eventually, the booting stage is completed when 50% of the ears have half emerged (Gate 1995). Booting is followed by heading step, stems elongation ends, and flowering occurs at the end of heading phase (Gate 1995).

Ripening corresponds to grain formation stages once flowering ends, while the senescence of green parts occurs. Grain development splits into two steps, milk development, and hard dough. Milk development occurs once the flowering is complete, the envelopes of future grains grow. The dough development represents the attainment of maximum dry weight with approximately 30 % moisture content. This stage is also known as physiological maturity. (Gate 1995). Eventually, ripening complete, the seed moisture will decrease down to 13 to 14 % (Wise et al. 2011; Gate 1995).

1.2 Remote sensing - Sentinel2

Sentinel-2 (S2) is the second high-resolution multispectral imaging mission of Copernicus Mission . It consists of a constellation of two polar-orbiting satellites placed in the same sun-synchronous orbit, phased at 180° to each other. The mission objective is monitoring variability in land surface conditions and satellite wide swath width (290 km) and allows a high revisit time (2 satellites under cloud-free conditions results in 2-3 days cycles at mid-latitudes).

Sentinel-2 satellites are equiped with a MultiSpectral Instrument (MSI). The MSI captures the light reflected by the Earth and separates the different wavelengths using specific filters. Three types of resolution characterize the information recorded by the sensor of a Sentinel-2 satellite. The purpose of each spectral band and its raw resolution is summarised in Table 1.1.

Table 1.1: Sentinel2 Bands and their original purpose - (GDAL 2019)

Band	Range	Resolution (m)	Central wavelength (nm)	Band width (nm)	Purpose
B01	Visible	60	443	20	Aerosol detection
B02		10	490	65	Blue
B03		10	560	35	Green
B04		10	665	30	Red
B05	Red-Edge	20	705	15	Vegetation classification
B06		20	740	15	
B07		20	783	20	
B08	NIR	10	842	115	Near infrared
B08A	NIR narrow	20	865	20	Vegetation classification
B09	SWIR	60	945	20	Water vapour
B10		60	1375	30	Cirrus
B11		20	1610	90	Snow / ice /
B12		20	2190	180	cloud discrimination

1.3 Introduction to biophysical vegetation variables

The different spectral range corresponds to different information in terms of vegetation classification and phenology. Visible bands corresponds to absorption bands of pigments that resides in outer palisade leaf (Chlorophyll pigments,carotene, Xantholphyll), (Eumetrain.org 2018)

The infrared lights splits into different subranges. NIR is mainly reflected by leaf internal structure [1] (Eumetrain.org 2018). Red-edge is the transition zone of the vegetation reflectance spectrum between visible and NIR. The absorption of radiation by water has a dominant influence on SWIR reflectance, but cellulose and lignin also absorb radiation in this range.

FCOVER, LAI & FAPAR

Despite this work mainly focus on FCOVER, many different ways exists to characterize the canopy chlorophyll content, each of one having its own meaning and sensitivity to environmental parameters. (Weiss 2019) provides a summary of how these different variables are used in agronomy, FCOVER is mainly used to asses evapotranspiration of crops, other variables are used to directly study the evolution of carbon balance in the system by studying

[1] It consists of spongy mesophyll cells located in the leaves' interior or back

respiration/phytosynthesis, while LAI is also used to study nitrogen cycle in crops (Jay et al. 2017; Liu et al. 2018) Compared to other vegetation indices, FCOVER has the advantage to have a quasi-linear relation with reflectances and a lower scale dependence than other indicators (Weiss 2020).

Table 1.2: Summary - a) crop processes and their variables of interest - (Weiss 2019), b) Relationship between variables and measurement parameters - (Weiss 2020)

(a)

Crop processes	LAI	FAPAR	FCOVER
Photosynthesis	+++	+++	
Evapotranspiration	++	+++	+++
Respiration	++		
Nitrogen	+++		
Phenology	+++	++	

(b)

	Sensitivity/Dependence			
Variable	Orientation	Scale	Reflectances	Observation conditons
LAI	Yes	Strong	Non-Linear	No
FAPAR	Yes	Strong	Non-Linear	Yes
FCOVER	-	Weak	Quasi-Linear	No

(Weiss 2020) defines LAI as half the developed area of photosynthetically active elements of the vegetation per unit horizontal ground area. According to Weiss 2020, it provides a proxy for the size of the exchange interface for energy (including radiation) and mass transfers between the canopy and the atmosphere.

FAPAR corresponds to the fraction of photosynthetically active radiation absorbed by the canopy (Weiss 2020). Thus, the FAPAR value results directly from the radiative transfer in the canopy, which is instantaneous. It depends on canopy structure, vegetation element optical properties and illumination conditions. Usually FAPAR values are integrated on a time scale.

Fractional vegetation cover) is generally defined as the ratio of the vertical projection area of above-ground vegetation organs on the ground to the total vegetation area. FCOVER is

used to separate vegetation and soil in energy balance processes, including temperature and evapotranspiration (Weiss 2020).

1.4 Fraction of green Vegetation Cover - Monitoring Methodologies

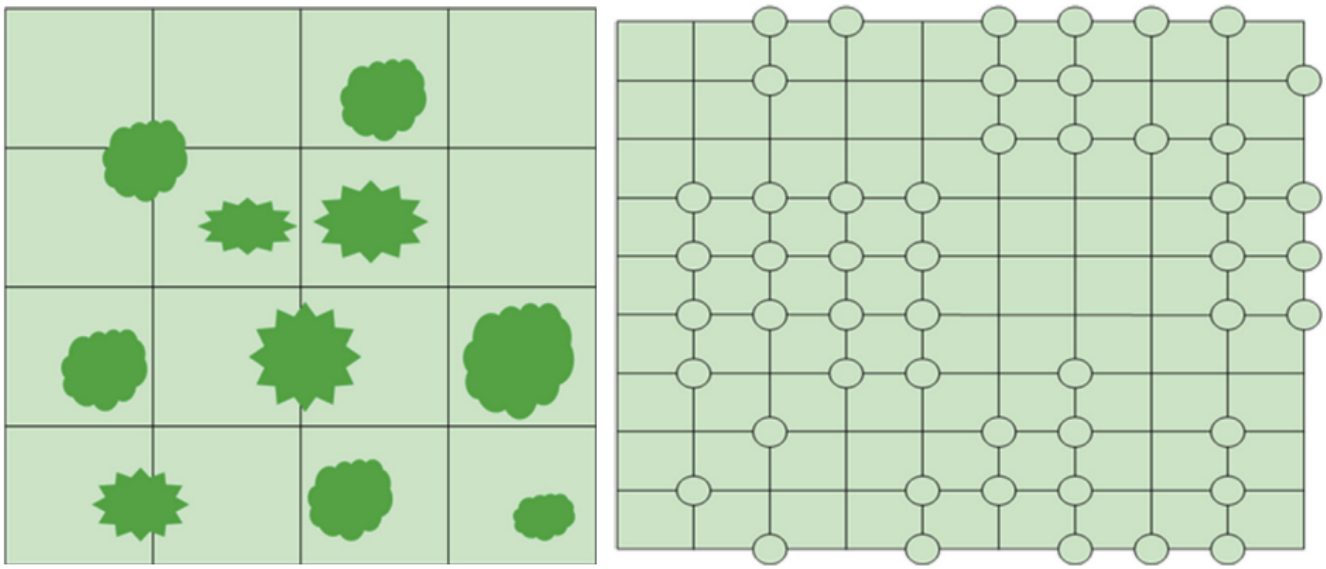

(a) (b)

Figure 1.2: Example of sampling grid historically used to perform field FCOVER measurement (Liang and Wang 2020)- a) FCOVER is given as the proportion of the corners of the grid that that touch vegetation, b) FCOVER is given by the proportion of grid cells where a bush is present

Historically, agronomists performed FCOVER measurement based on sampling methods on field, what is shown on Figure 1.2, using statistical methods to upscale FCOVER estimations at the scale of a parcel (Carpenter et al. 1999). These methods were initially based on visual estimation, which added a huge subjectivity component (Liang and Wang 2020). Currently, thanks to the advent of numerical photography and UAV technologies, FCOVER estimations grew out of these subjectivity factor.

Table 1.3: Indicators used into optical measuring methods

Name	Color Space	Symbol	Indicator	
Green Component	RGB		G	(1.2)
Green Excess	RGB	EGI	$2G - R - B$	(1.3)
Green Excess	RGB	EG	$\min(G - R, G - B)$	(1.4)
Greenness	LAB		a	(1.5)

Optical measuring instruments

Optical measurement are the most direct ways to provide an estimation of FCOVER using field measurement. (Liang and Wang 2020) recommends to select carefully the moment at which photographs are taken, illumination conditions should be selected. A cloudy day, the morning or the evening are the moment at which the the effect of shadows is minimal. Morning dew might also affect the photography,so early morning is not recommended. Different kind of images can be used : RGB and Multispectral. Multispectral sensors additional bands have usually a biophysical meaning for vegetation, NIR or Red-edge. Post-acquisitipn procedure can involve a segmentation step at which a methodology is used to separate green vegetation from soil background.

The post-acquisition process is crucial, and this step consists of image segmentation; it consists of classifying pixels into multiple classes to partition images into regions sharing similar classes. In the case of FCOVER, classes are the vegetation and the soil. FCOVER of an image (or a window of a given size in an image) is computed by computing the proportion of vegetation pixels over the complete size of the mask, what is expressed by (1.1).

$$\text{FCOVER} = \frac{\#_{Vegetation}}{\#_{Pixels}} \tag{1.1}$$

Vegetation detection is usually related to color components and color components information has to be summarized preferentially in one value. Most basic applications select the reflectance band associated to green, but there exist multiple ways to summarize information. Table 1.3 describes different proxies of greenness that are used to implement FCOVER estimators.

Supervised segmentation requires human intervention by manually selecting criteria based on color or creating training datasets. Unsupervised methods create classes automatically, but the computational cost of unsupervised methods is usually higher, while interpretation

Table 1.4: Some Vegetation Indices used in crop modelling - (Heidarian Dehkordi et al. 2020)

Index Name	Symbol	Formula)	
Normalized difference vegetation index	NDVI	$\frac{\rho_{\text{nir}} - \rho_{\text{red}}}{\rho_{\text{nir}} + \rho_{\text{red}}}$	(1.6)
Green normalized difference vegetation index	GNDVI	$\frac{\rho_{\text{nir}} - \rho_{\text{green}}}{\rho_{\text{nir}} + \rho_{\text{green}}}$	(1.7)
Weighted difference vegetation index	WDVI	$\rho_{\text{nir}} - a\rho_{\text{red}}$ where $a = \frac{\rho_{\text{nir}-\text{soil}}}{\rho_{\text{red}-\text{soil}}}$	(1.8)
Normalized difference red edge index	NDRE	$\frac{\rho_{\text{nir}} - \rho_{\text{red-edge}}}{\rho_{\text{nir}} + \rho_{\text{red-edge}}}$	(1.9)
Optimized soil adjusted vegetation index	OSAVI	$1.16\frac{\rho_{\text{nir}} - \rho_{\text{red}}}{\rho_{\text{nir}} + \rho_{\text{red}} + 0.16}$	(1.10)
Chlorophyll vegetation index	CVI	$\frac{\rho_{\text{nir}}}{\rho_{\text{green}}} \frac{\rho_{\text{red}}}{\rho_{\text{green}}}$	(1.11)
Enhanced vegetation index	EVI	$2.5\frac{\rho_{\text{nir}} - \rho_{\text{red}}}{\rho_{\text{nir}} + 6\rho_{\text{red}} - 7.5\rho_{\text{blue}} + 1}$	(1.12)
Chlorophyll index red	$\text{CI}-\text{red}$	$\frac{\rho_{\text{nir}}}{\rho_{\text{red}}} - 1$	(1.13)
Simplified canopy chlorophyll content index	sCCCI	$\frac{\text{NDRE}}{\text{NDVI}}$	(1.14)

of the results is sometimes complex and depends on the selected algorithm. Figure 1.3 shows how the segmentation masks and FCOVER can vary in the case of unsupervised methods applied on similar images.

k-means and ISODATA consist of iterative clustering algorithms (Merzougui et al. 2016). During the initial step, cluster centroids are assigned, potentially randomly. Then distances to cluster centroids are computed, and points are classified into the cluster of the nearest centroid at the end of the second step. Next, new cluster centroids are calculated from existing centroids. The second step is repeated until "change" between iterations becomes negligible. Process can be repeated by varying initialization of centroids to determine the robustness of the result. The difference is that k-means use a definite number of k classes, while ISODATA merges or split clusters depending on the distance of the centroids or the number of pixels of each class. k-means and isodata can be slow compared to other algorithms but adding additional classes is simple to consider heterogeneities in images.

Image processing widely uses the Otsu algorithm; a threshold is selected to split 2 classes according to a histogram. The objective is to minimize (resp. maximize) intraclass (resp.

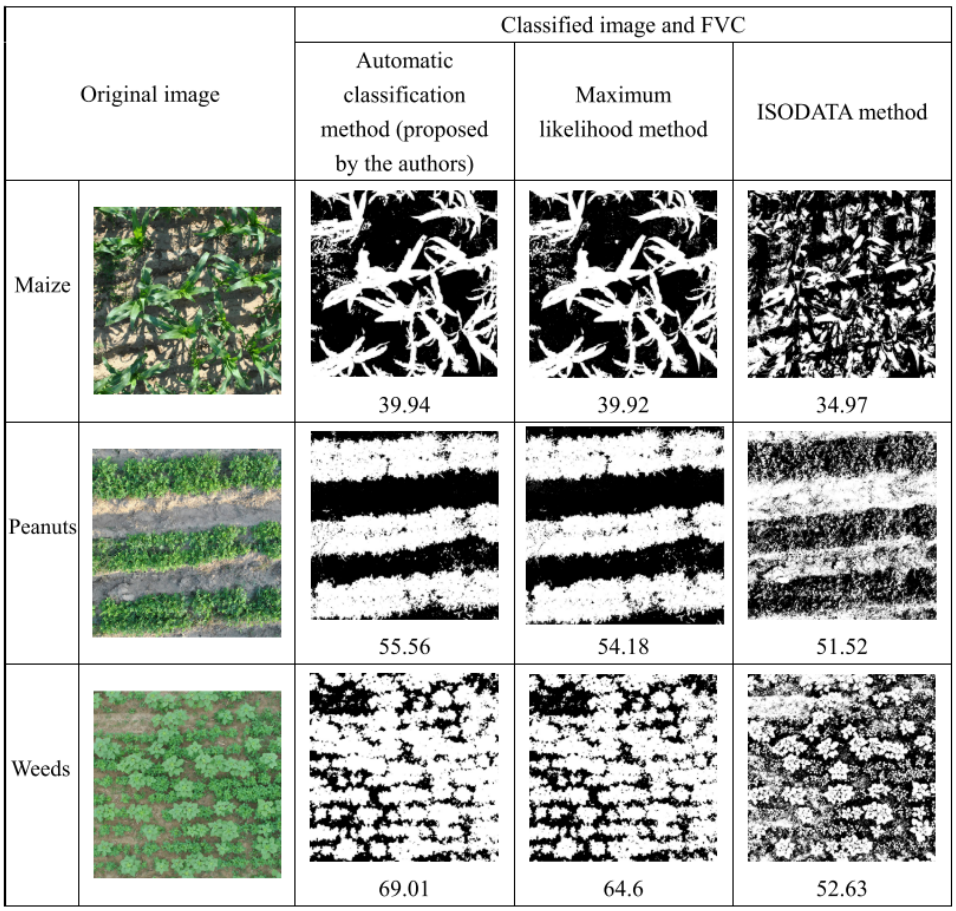

Figure 1.3: Comparison of the classification results using different classification methods. (Liang and Wang 2020)

interclass) variance (Bangare et al. 2015). Maximum likelihood assumes that vegetation and soil pixels follow two normal distributions of different (and unknown) means and standard deviation. A regression algorithm is used to estimate the values of normal distribution parameters (Raschka 2015). A threshold is finally selected to minimize misclassification probabilities according to normal distribution parameters. In the assumption of normal distribution, this threshold is located at the intersection of both curves. On the contrary of iterative algorithms, Otsu and maximum likelihood algorithm computational cost is low, while the simplicity of the results often can't take efficiently take into account shaded or saturated parts of a canopy (Utstumo et al. 2018).

Shadows or surexposition affects strongly segmentation processes. (Song et al. 2015) constructs a shadow resistant algorithm, this algorithm is based on a brightness correction of the shaded part of the image and use a linear combination of a lognormal distribution and

a normal distribution to approximate greenness histogram, to finally segment green vegetation the background to finally apply a maximal likelihood algorithm under new assumptions on distribution. (Sadeghi-Tehran et al. 2017) developed a supervised algorithm dedicated to RGB images, it derivates 21 color components (including colinear variables) representation where a randomforest classifier is trained using images presenting a strong probability of heterogeneity.

RGB - Photography at low altitude (<2m)

Low altitude photography provide an accurate estimation on a reasonable surface. Photography at low altitude are usually either used as a part of a sampling method to characterise FCOVER at a larger scale or to produce training datasets for different methods based, what is show on Figure 1.4. CANEYE is a project where hemispherical pictures of crops are collected and segmented to train an algorithm able to provide a fast prediction of FCOVER. These calibration segmented images are also used to train some remote sensing retrieval algorithm.

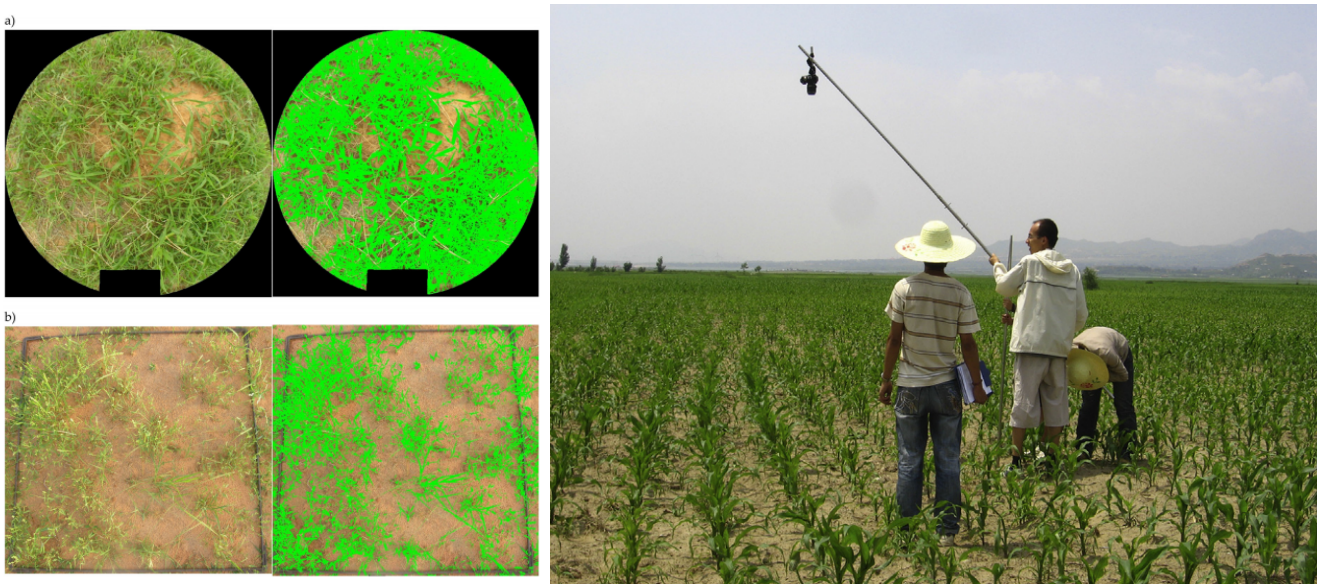

(a) (b)

Figure 1.4: Examples of manual photography acquisition - a)Caneye project, calibration images from (Mougin et al. 2018), b) example of low altitude acquisition set-up (Liang and Wang 2020)

Currently mobile phenotyping platform such as (Sadeghi-Tehran et al. 2017; Utstumo et al. 2018) allows to automatically collect RGB images at the scale of a parcel and eventually compute high precision FCOVER maps.

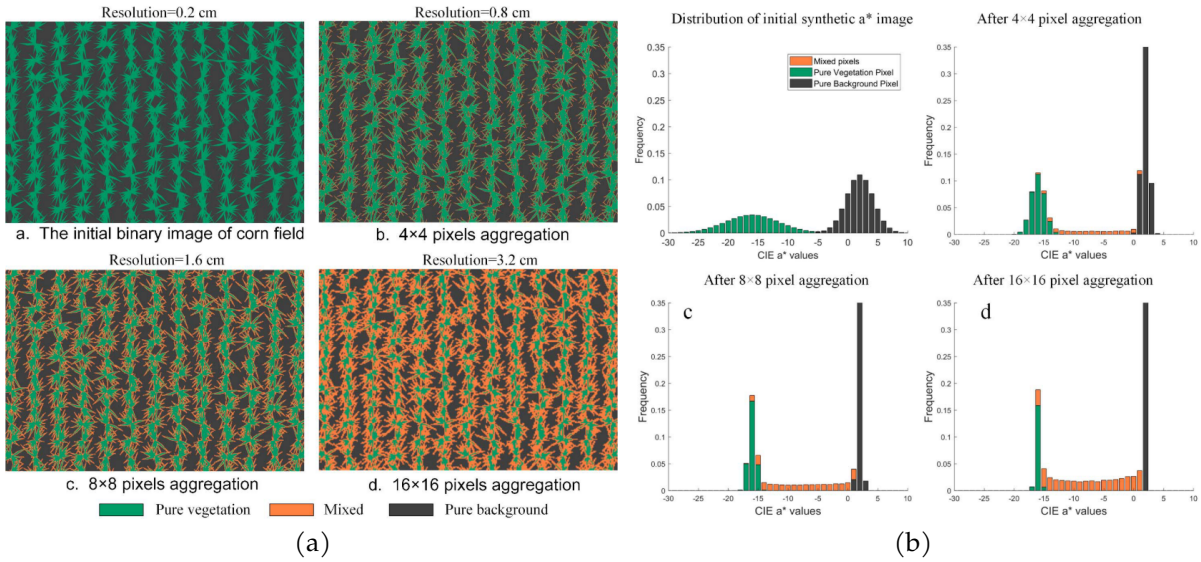

Figure 1.5: Influence of the resolution on mixed pixel, synthetic images (L. Li et al. 2018) -a) location of mixed pixels and b) proportion of mixed pixels as a function of spatial resolution

UAV - Image analysis analysis based method

UAV acquisition process aims to cover a larger area than photography at low altitudes. UAV images are taken from a high altitude, so the different images are merged using a processing chain to produce a mosaic. Segmentation methods developed for low-altitude pictures are currently widely used; But depending on the resolution of the final results and the crop characteristics, they produce biased results : on the contrary of low altitude pictures, the assumption that pixels represent bare soil or completely covered areas isn't always valid. The coarser is the resolution, the higher is the proportion of mixed pixels (L. Li et al. 2018). Figure 1.5 illustrates this trend using synthetic images aggregated at different resolution; mixed pixels proportion increases dramatically and greenness histograms are highly changed by resolution; Bimodal continuous distribution of pure pixels gradually change to a uniform distribution of mixed pixels on between two peaks representing pure pixels.

(L. Li et al. 2018) adress this problem of mixed pixels by fitting the histograms of pure vegetation pixels and pure background pixels are firstly fit using two half-Gaussian even this procedure solve the mixed problem for low altitude flight, extreme cases are still difficult to process.

Inversion of Radiative Transfer Models

Radiative Transfer Models (RTM) are used to model the reflectance of canopies depending on various parameters depending on canopy architecture and leaf characteristics, such as PROSAIL [2]. (Baret and Buis 2008; Berger et al. 2018). In RTM, Canopy architecture-related variables are LAI, Average leaf inclination angle, Soil reflectances/brightness factor, the fraction of diffuse illumination, and Sun zenith angle. The description of the leaves relies on mesophyll structure, dry matter, water, and pigment content [3] (Baret and Buis 2008; Berger et al. 2018). The computation process is summarized on Figure 1.6.

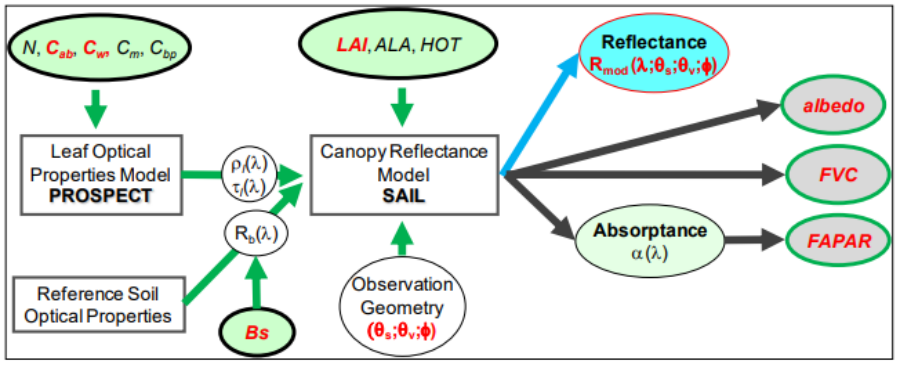

Figure 1.6: PROSAIL - Calculation of canopy reflectance - Schematic View (Berger et al. 2018) C corresponds to pigment abundance, N to the mesophylle geometric, θ_s to sun zenith angle, θ_v view zenith angle, ALA is the average leaf inclination angle, Hot, the Hotspot parameter and Bs describes soil properties (reflectance, wet or not), λ is the wavelength, ρ the reflectance and τ the transitivity

Currently, these models are coupled to inversion models to associate spectral canopies to a set of values for the parameters mentioned above, as stated by . Usually, pigments contents and the internal structure of the leaves have to be assumed to predict LAI (Duan et al. 2014; Wan et al. 2021). Eventually, LAI is transcripted to fCover using a beer-lambert equation given at (1.15) taking into account viewing zenith angles θ and the canopy's structure in parameter $G(\theta)$ (Wan et al. 2021; Fang 2015).

$$\text{FCOVER} = 1 - e^{-G(\theta)\frac{\text{LAI}}{\cos(\theta)}} \tag{1.15}$$

[2] PROSAIL is the most used radiative model in agronomy, emerging from two initially distinct projects optical modelization projects : PROSPECT (leaves optical parameters), and SAIL4 (canopies) (Baret and Buis 2008)

[3] Chlorophyll a + b, carotenoid, anthocyanin, brown pigments

Satellite Image - The remote sensing retrieval of FCOVER

Satellite Images doesn't offer a high enough resolution to perform predictions at the level of leave coverage, binary models developed in the case of optical sensors doesn't provide reliable results because most of pixels aren't pure bare soil or pure vegetation. Different strategies are developed to address this issue.

Linear and Non-Linear Model of Vegetation Indices

Historically, the first strategy is based on the fact that FCOVER has a quasilinear relation with Vegetation indices as normalized difference vegetation index (NDVI) or green normalized difference vegetation index (GNDVI). Usual strategy consists to detect bare soil pixels and fully covered pixels of a neighborhood, either using a supervised approach, either reference values of vegetation indices in literature or by assuming that local minimum (resp. maximum) of these vegetation indices are bare soils (fully covered) (Gutman and Ignatov 1998). If $a = 1$, (1.16) is linear, this is the most used form of this family of models.

$$\mathrm{FCOVER} = \left(\frac{\mathrm{NDVI} - \mathrm{NDVI}_{soil}}{\mathrm{NDVI}_{plant} - \mathrm{NDVI}_{soil}} \right)^{a} \tag{1.16}$$

a is sometimes selected with different values, (Gao et al. 2020) states that (1.16) can be quadratic while other models fixed a to 0.62. Other vegetation indices are used in regressions, but usually experimental datasets where FCOVER is computed using alternative methodologies are required to calibrate model.

Machine-Learning based methods

Machine-learning is widely used to retrieve Biophysical indices, one of the most used these last years is the sentinel2 toolbox developed by (Weiss 2020). This toolbox available in SNAP, a freeware edited by ESA allowing to compute vegetation indices directly from Sentinel2 Images. It relies on a neural network which is trained using synthetic datasets. These datasets are generated from Prosail, a radiative transfer model presented at subsection .

This neural net is based on a single layer of five neurons with tangent sigmoid transfer functions, 12 inputs, which means that 60 weights are required to calibrate the neural net

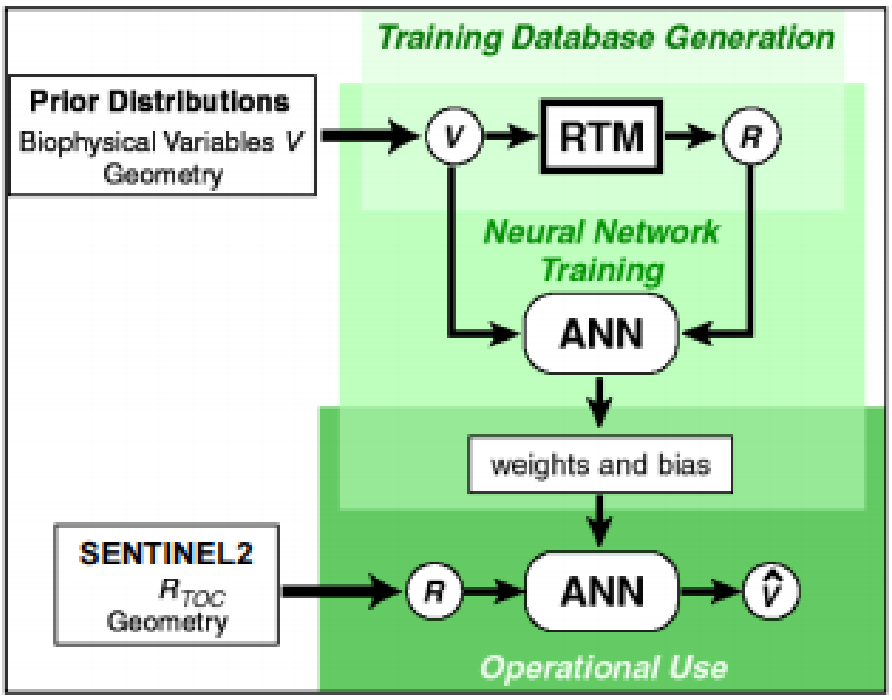

Figure 1.7: SNAP - Flowchart (Weiss 2020)

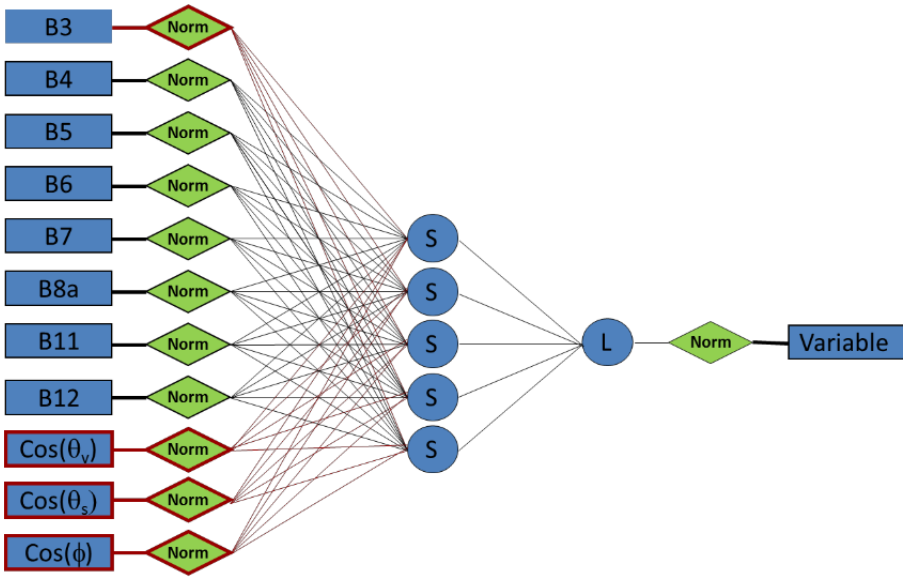

Figure 1.8: Achitecture of SNAP Neural net (Weiss 2020) - The inputs are differents bands available on sentinel2 datasets B3, B4, B5, B6, B7, B8a, B11, B12, viewing zenith, sun zenith and relative azimuth angle.

1.5 Canopy expansion Models

FCOVER Monitoring allows to generate timeseries and information of FCOVER timesrieshas to be summarized into a model, based on a reduced set of parameters in order to directly use it into a model able to describe yield and biomass production. These parameters have a biophysiological meaning.

If time is a natural way to describe canopy development, annual climate variations makes comparison often complicated, even at a same location. For this reason, agronomists use multiple proxies to transcript crop development rate as a numerical value; one of the most pragmatic and straightforward descriptions is written by (1.17) and (1.18).

$$\mathrm{GDD}_i = \max\left(0, \frac{T_{min-i} + T_{max-i}}{2} - T_{base}\right) \tag{1.17}$$

$$\mathrm{GDDc}(n_{Days}) = \sum_{i=1}^{n_{Days}} \mathrm{GDD}_i \tag{1.18}$$

T_{min-i} (resp. T_{max-i}) express daily minimal (resp.maximal) temperature, n_{Days} is the number of days after sowing. GDDc is called thermal time, and its units are $^{\circ}\mathrm{C\,d}$, while GDD_i is the daily average temperature on base T_b, it describes the daily contribution to plant development. (1.17) states that the temperature response of the development rate is a linear function of temperature; if the temperature falls below the base temperature T_b during a significant part of the day, the development rate is assumed negligible that day.

Simultaneous crop growth and climate monitoring on the field allowed establishing correspondences between crop phenological development and thermal time for the different crops and strains. Agronomists developed standardized scales to describe crop development; the most widely used scale in the cereal industry is the BBCH scale, where a two-figure code is associated at each development stage from germination to maturity.

Agronomists currently work on new proxies in crop modeling software, directly incorporating phenological characteristics of crops, for example, by adding penalty factors (1.17) or by including day length into the computation. The penalty factors allow decreasing development rate depending on vernalization, photoperiod, and temperature stress as development indicator introduced by (Rosillon et al. 2020).

This kind of model is summarized by the equation system available in Appendix A.2.

Mathematical formulations of Canopy Growth Cycle

Growth Cycle are studied using various variables, Table 1.5 provides a short summary of methodologies used to describe canopy expansion and senescence during a growing season.

Table 1.5: Examples of crop growth models used to model Ecosystem canopy expansion

Source	Growth Model Formulation	Context
(Richter and Seppelt 1996)	Differential Equation	Biomass production modelling as a function of nitrogen balance
(Fischer 1994)	Double logistic function	Crop monitoring
(Badeck et al. 2004; Doktor et al. 2009)	Linear Model by connecting maximal value to the beginning of growth cycle	Forest Canopy
(Zhang et al. 2003; Soudani et al. 2008)	Double sigmoidal function	Ecosystem monitoring
(Myers et al. 2019)	Piecewise logistic function	Crop Monitoring

Mechanistic model developed by (Richter and Seppelt 1996) is formulated as a differential system describing biomass production W as a function of growth rate, N nitrogen resources consumption, senescence f_s and fertilizer inputs U. Similar models are applied to FCOVER expansion. This kind of mechanistic model allows to represent a complete growth cycle as a function of resources, but there isn't any simple explicit equation to perform regression on FCOVER measurements.

$$\dot{W} = r_{\max} r(N) f_s(\mathrm{GDDc}) W - \mu W \tag{1.19}$$

$$r(N) = \frac{N}{N + k_R} \tag{1.20}$$

$$f_s(t) = \frac{\alpha \mathrm{e}^{-\rho\,\mathrm{GDDc}}}{1 + \alpha \mathrm{e}^{-\rho\,\mathrm{GDDc}}} \tag{1.21}$$

$$\dot{N} = -d(W, \mathrm{GDDc}) - k_l N + k_m \mu \dot{W} + U(\mathrm{GDDc}) \text{ with } N(0) = N_0 \tag{1.22}$$

$$U(\mathrm{GDDc}) = \sum_{i=1}^{p} u_i \delta\left(\mathrm{GDDc} - \mathrm{GDDc}_i\right) \tag{1.23}$$

Explicit equations are required to perform efficient regression on parameters and interpret the results. (Fischer 1994; Zhang et al. 2003; Soudani et al. 2008) models are quite similar despite mathematical formulations vary, growth functions have at least six parameters to be fitted and equations are provided on a continuous domain. Double logistic function is described by (1.5), this function is continuously derivable and continuous but the number of

parameters imposes a high number of observations to fit the model. CC_b is the baseline, CC_a represents the amplitude and CC_e is the value at the end of growing season. GDDc_i (resp. GDDc_d) describes when the maxima increase (resp. decrease) occurs, p (resp. q) is related to the slope at this the thermal time. k is a parameter.

$$\mathrm{CC}(\mathrm{GDDc}) = \mathrm{CC}_b + \frac{k}{1+\exp(-p(\mathrm{GDDc}-\mathrm{GDDc}_i))} - \frac{k+\mathrm{CC}_a-\mathrm{CC}_e}{1+\exp(-q(\mathrm{GDDc}-\mathrm{GDDc}_d))} \quad (1.24)$$

(Myers et al. 2019) provides a generalisation of double logistic/sigmoid where growth curve is fitted on piecewise domain. Parameters are very similar to , but approach is repeated on four distinct domains are defined on Figure 1.9. On each of them GDDc_{i-j} (resp. GDDc_{d-j}) is the thermal time associated to maximal increase (resp. decrease).

$$\mathrm{CC}(\mathrm{GDDc}) = \mathrm{CC}_b + \frac{1}{2}\,\mathrm{CC}_a\left[\tanh\left(p\cdot(\mathrm{GDDc}-\mathrm{GDDc}_{i-j})\right) - \tanh\left(q\cdot(\mathrm{GDDc}-\mathrm{GDDc}_{d-j})\right)\right] \quad (1.25)$$

Looking for these characteristic points requires to approximate second derivatives.

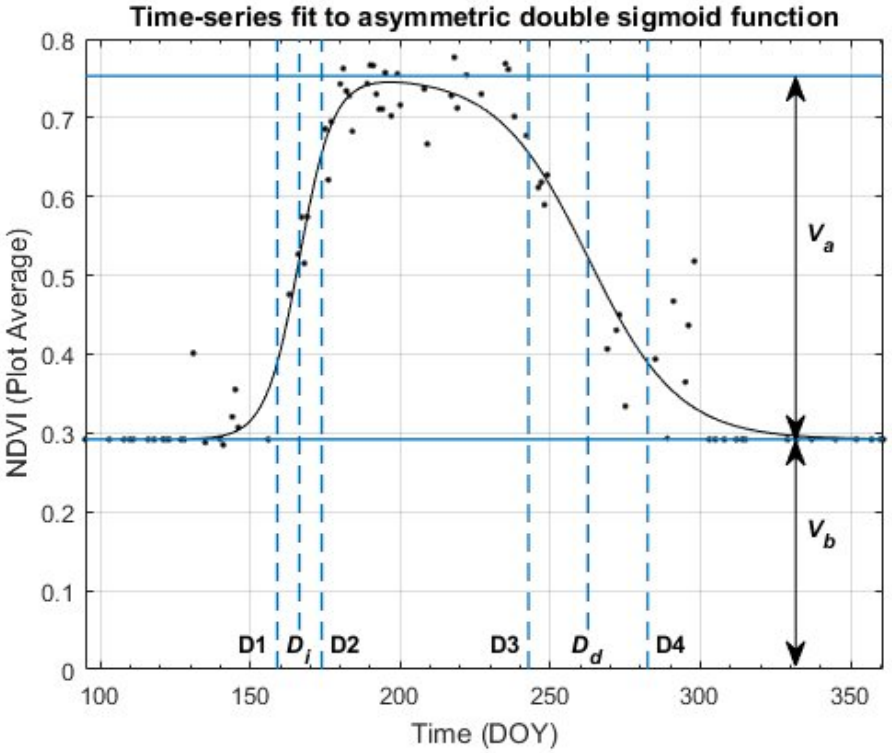

Figure 1.9: (Myers et al. 2019) - Piecewise logistic function - Geometrical interpretation of the parameters

Aquacrop uses an alternative piecewise representation using exponentials on different intervals, which is close to a double sigmoid representation. This representation is continous and derivable and offering a simplified representation that can be easily linked to the phenology of crops that are studied using a reduced number of parameters that directly have a physiological meaning.

Table 1.6: FCOVER Piecewise Exponential Model - Aquacrop

CC		Range	Phase
0	(1.26)	$[0; \mathrm{GDDc}_0]$	Emergence
$\mathrm{CC}_0 \exp(\mathrm{CGC}(\mathrm{GDDc} - \mathrm{GDDc}_0))$	(1.27)	$[\mathrm{GDDc}_0; \mathrm{GDDc}_{50\%}]$	Exponential Growth
$\mathrm{CC}_x \left[1 - 0.25 \frac{\mathrm{CC}_x}{\mathrm{CC}_0} \exp(-\mathrm{CGC}(\mathrm{GDDc} - \mathrm{GDDc}_0))\right]$	(1.28)	$[\mathrm{GDDc}_{50\%}; \mathrm{GDDc}_{max}[$	Exponential Decay
CC_x	(1.29)	$[\mathrm{GDDc}_{max}; \mathrm{GDDc}_{Sen}]$	Maximum Cover
$\mathrm{CC}_x \left[1 - 0.05 \left\{\exp\left(3.33 \frac{\mathrm{CDC}(\mathrm{GDDc} - \mathrm{GDDc}_{Sen})}{\mathrm{CC}_{x0} + 2.29}\right) - 1\right\}\right]$	(1.30)	$[\mathrm{GDDc}_{Sen}; \mathrm{GDDc}_{End}]$	Decline
0	(1.31)	$[\mathrm{GDDc}_{End}; +\infty[$	Maturity/ Post-Harvest

Implicit parameters $\mathrm{GDDc}_{50\%}$ and GDDc_{End} are computed as :

$$\mathrm{CC}(\mathrm{GDDc}_{50\%}) = \frac{\mathrm{CC}_x}{2} \longrightarrow \mathrm{GDDc}_{50\%} = \mathrm{GDDc}_0 + \frac{1}{\mathrm{CGC}} \ln\left(\frac{\mathrm{CC}_x}{2\,\mathrm{CC}_0}\right) \tag{1.32}$$

$$\mathrm{CC}(\mathrm{GDDc}_{End}) = 0 \longrightarrow \mathrm{GDDc}_{End} = \mathrm{GDDc}_{Sen} + \frac{\mathrm{CC}_{x0} + 2.29}{3.33\,\mathrm{CDC}} \ln(21) \tag{1.33}$$

Model explicit parameters are defined as

- GDDc_0 : thermal time at 90% of the emergence
- GDDc_{Sen} : thermal time at start of the senescence
- CC_x : maximal canopy cover that can be reached [-]
- CC_0 : Canopy Cover at 90% of the emergence [-]
- CGC : Canopy Growth Coefficient $[(°\mathrm{Cd})^{-1})]$
- CDC : Canopy Decline Coefficient $[(°\mathrm{Cd})^{-1})]$

An interpretation of these six parameters is provided on Figure 1.10. Growth is splitted into five thermal time intervals.

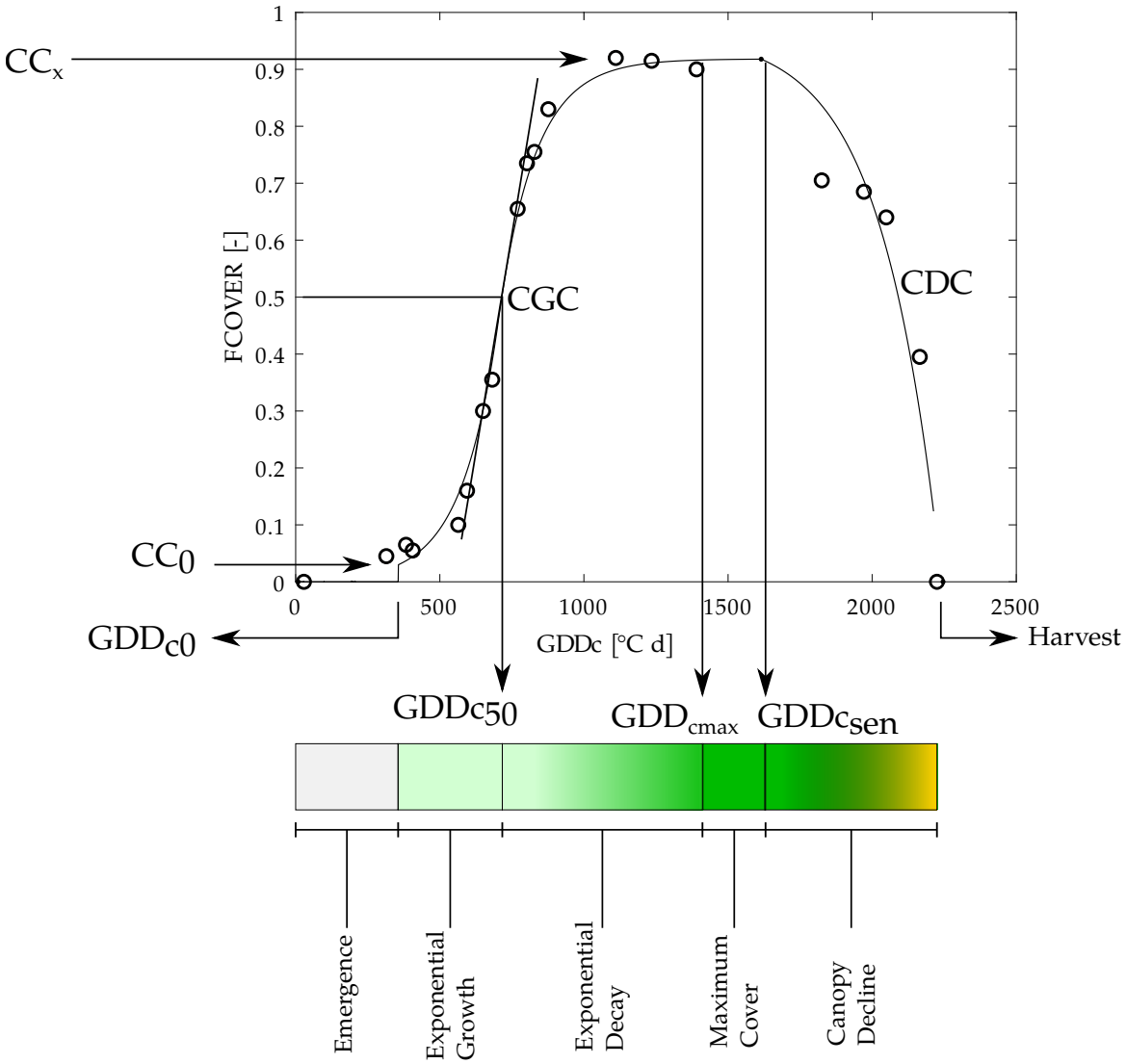

Figure 1.10: FCOVER as a function of thermal time - Aquacrop Model

Model states that soils is completemy bare during emergence. This period is followed by exponential growth which includes tillering and stem elongation, which corresponds to (1.27). Exponential decay corresponds to a decrease of growth rate, as stated by (1.28). This step occurs simultaneously to the beginning of inflorescence formation. Flowering occurs during the maximum canopy cover, which is followed by senescence. Ripenning occurs during the senescence, what is modeled by (1.30). The most import parameter to estimate is implicit : $\mathrm{GDDc}_{50\%}$ is the thermal time at which the maximal growth rate, which equals to CGC occurs, it corresponds to an inflexion point. It also determines the transition time between exponential growth and decay.

1.6 Yield and biomass production modeling

Currently, yield and biomass production have been modeled of winter wheat is using various software (Palosuo et al. 2011).

Yield production shows a strong correlation with the integral of FCOVER, which can be written using (1.27), (1.28), (1.29), and (1.30), what is written in Appendix A.1

$$Y \propto \int_0^{\mathrm{GDDc}_{End}} \mathrm{FCOVER}\,\mathrm{d}\,\mathrm{GDDc} \tag{1.34}$$

$$\begin{aligned} &\propto \frac{0.5\,\mathrm{CC}_x - \mathrm{CC}_0}{\mathrm{CGC}} + CC_x\left[\mathrm{GDDc}_{max} - \mathrm{GDDc}_{50\%}\right] + \\ &0.25\frac{\mathrm{CC}_x}{\mathrm{CGC}}\left[1 - e^{-\,\mathrm{CGC}(\mathrm{GDDc}_{max} - \mathrm{GDDc}_{50\%})}\right] + \\ &\mathrm{CC}_x\left(\mathrm{GDDc}_{sen} - \mathrm{GDDc}_{max}\right) + \mathrm{CC}_x(0.95\ln 21 - 1)\frac{\mathrm{CC}_{x0} + 2.29}{3.33\,\mathrm{CDC}} \end{aligned} \tag{1.35}$$

Aquacrop Model

AquaCrop is water driven model simulating crop productivity and yield edited by FAO. Crops are modeled as an ecosystem split into different functional subsystems exchanging water according to environmental conditions (Wellens et al. 2014). The model separates non-productive consumption (soil evaporation, runoff, infiltration) from the productive consumption of water (transpiration) (Steduto et al. 2013).

It allows modeling crop growth-related variables, such as Canopy cover, biomass accumulation, and yield, and many others such as water flux and water content in root zone layers, crop transpiration. Compared to other crop growth modeling software, Aquacrop uses either robust models or semi-empirical equations based on easily measured parameters to offer a pragmatic approach to agronomists.

Following (Wellens et al. 2014), inputs of the model are divided into four categories: climate, soil properties, crop characteristics and crop management. Aquacrop requires a reduced amount of climate variables daily, air temperature, precipitations, the potential evapotranspiration ET_0, and carbon dioxide concentration. ET_0 is , which can be computed using the Penman-Monteith equation. Soil properties are defined by horizons, which are splited into layers of given thickness whose properties are water content at wilting point, water content at saturation, water content at field capacity, conductivity at saturation, and drainage characteristics. Crop characteristics include the start of the growing cycle, the production,

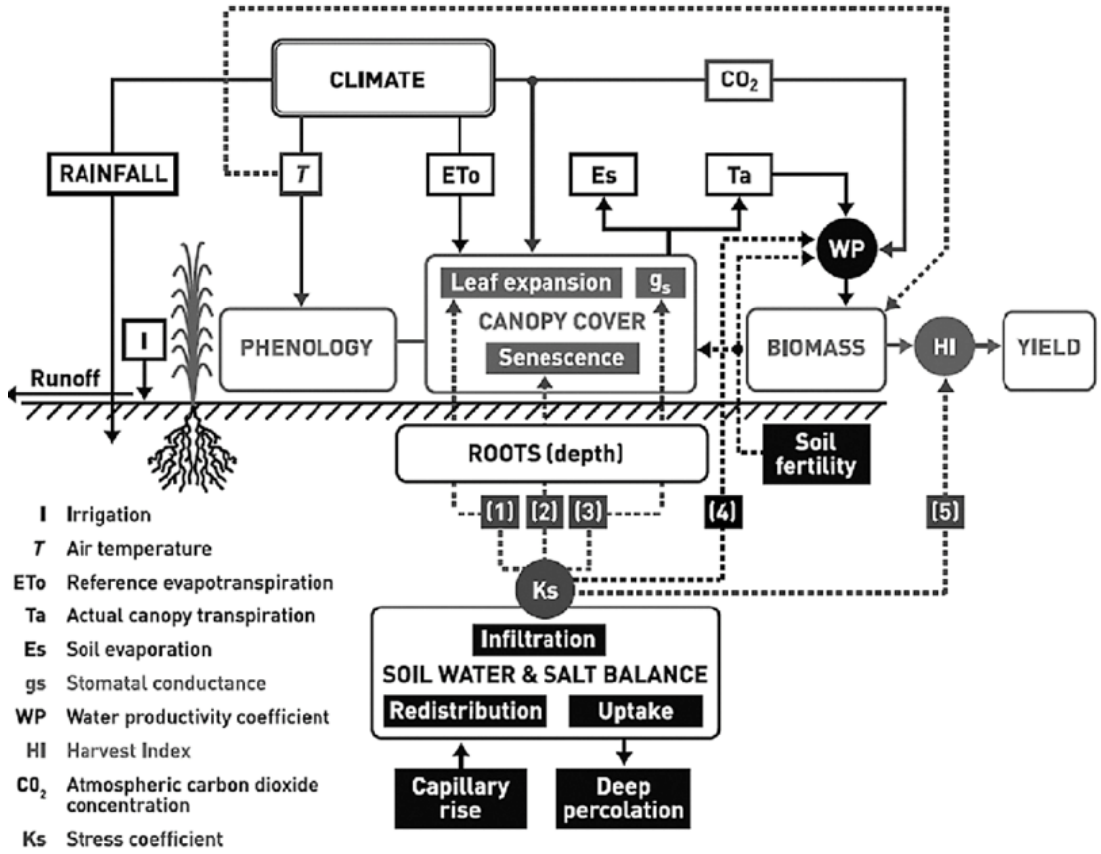

Figure 1.11: Aquacrop - Systemic view - (Steduto et al. 2013)

evapotranspiration parameters, stresses (water, fertility, temperature), calendar of the growing process. Management operations affecting growth are either irrigation (irrigation schedule and method can be fixed) or field management (fertilization, mulches, field surface practices – runoff control, soil bunds). However, the consequences of pests, diseases, or weeds on the crop are not considered.

Water exchange between subsystems and crop growth related variables are computed using the different modules shown at Figure 1.11. Roots depth and Canopy cover are considered as independent modules. Phenology describes growth rate of the canopy as a function of thermal time and how canopy cover reacts as a function of plant development to different kind of stress and potential early senescence that could be transcripted by a reduced canopy development compared to theoretical model fixed by user inside crop parameters. Water balance module allows to quantify total available water in root layers and how water fluxes evolves as a function of climate and plant development.

$$T_r = K_S \cdot \mathrm{CC} \cdot K_C \cdot \mathrm{ET}_0 \tag{1.36}$$

$$B = \mathrm{WP} \sum_{i}^{N_{Days}} T_r \tag{1.37}$$

$$Y = \mathrm{HI}_0 \, f_{\mathrm{HI}}(\mathrm{GDDc}) \cdot B \tag{1.38}$$

$$f_{\mathrm{HI}} = \min \left[\max \left(0, \frac{\mathrm{GDDc} - \mathrm{GDDc}_{min-YF}}{\Delta_{YF}\,\mathrm{GDDc}} \right), 1 \right] \tag{1.39}$$

$$\tag{1.40}$$

T_r represents crop transpiration [mm]
B is the accumulated biomass $[\mathrm{kg/m^2}]$
ET_0 is the reference evapotranspiration [mm/d], it describes the atmospheric evaporative demand as stated by (Vavlas et al. 2020).
K_c is the mid-season crop coefficient, which can be adjusted for crop ageing and possible adverse early senescence effects (Steduto et al. 2013).
K_S describes the soil water crop coefficient integrating water logging, stomatal closure and early senescence effects (Steduto et al. 2013).
WP is the water productivity parameter $[\mathrm{gm^{-2}mm^{-1}}]$).
HI_0 is the reference harvest index at the physiological maturity of the crop.

Preponderant equations describing crop growth are summarised by (1.36), (1.37), (1.38) and (1.39).

WP considered as a conservative parameter, independent from climate and depending mainly from carbon dioxide concentration (Steduto et al. 2013). Yield formation is a described using a factor varying varying linearly from zero to one as a function of thermal time, which is written in (1.39). It starts when crop overreach GDDc_{min-YF} and reaches its maximal value after a given amount of thermal time $\Delta_{YF}\,\mathrm{GDDc}$. Figure 1.12 shows a systemic view of Aquacrop, showing feedbacks of the system to incorporate water stresses to the model and adding early senescence effects to the model.

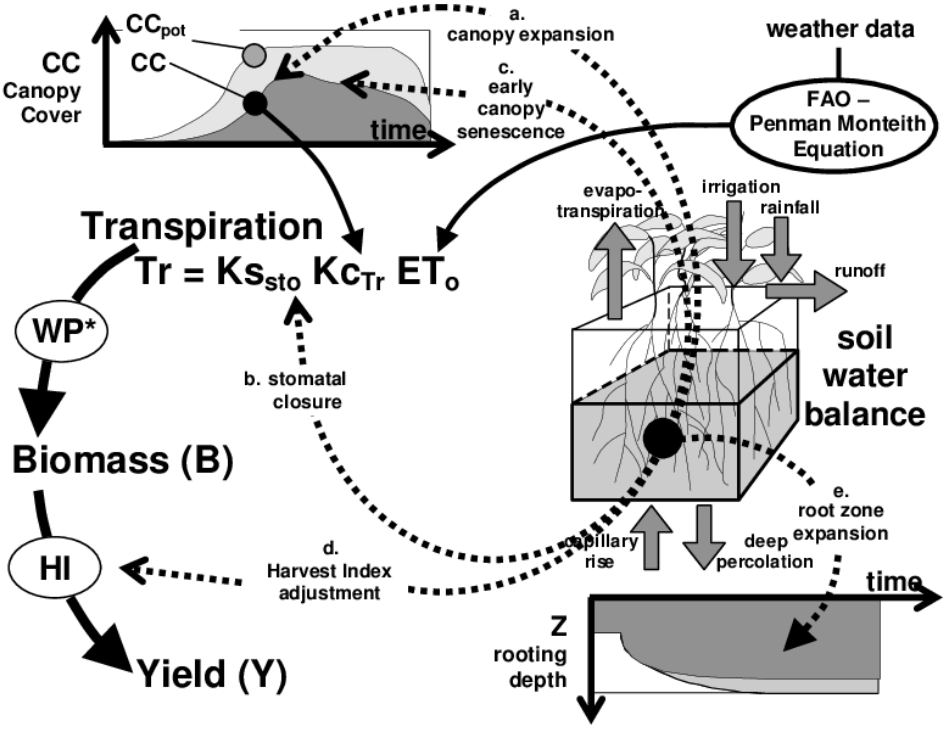

Figure 1.12: Aquacrop Flowchart - Water Balance

Comparison with other existing Biomass production modeling

(Palosuo et al. 2011) provides a benchmark of different models describing winter wheat crop growth using alternatives of Aquacrop. (Palosuo et al. 2011) performed modelisation during 49 growing seasons at eight sites in northwestern. Table 1.7 lists multiple models that are widely used to model winter wheat growth. (Palosuo et al. 2011) provides a comparison and Aquacrop is added to these models. Most of these are mechanistic and describes photosynthesis and respiration processes.

Table 1.7: Existing producing models tested in the case of Winter Wheat, adapted fom (Palosuo et al. 2011)

Model	Version	Description	Web address
APES	V. 0.9.0.0	(Wien et al. 2010)	http://www.apesimulator.it
CROPSYST	V. 3.04.08	("CropSyst, a cropping systems simulation model" 2003)	http://modeling.bsyse.wsu.edu
DAISY	V. 4.01	(Abrahamsen and Hansen 2000)	https://daisy.ku.dk
DSSAT	V. 4.0.1.0	(Jones et al. 2003; Hoogenboom et al. 2012)	https://dssat.net
FASSET	V. 2.0	(Berntsen et al. 2003; Doltra, Lægdsmand, and Olesen 2011)	http://www.fasset.dk
HERMES	V. 4.26	(Kersebaum 2007)	Request from ckersebaum@zalf.de
STICS	V. 6.9	("STICS: a generic model for simulating crops and their water and nitrogen balances. II. Model validation for wheat and maize" 2002)	http://www.avignon.inra.fr/agroclim stics eng/
WOFOST	V. 7.1	(Boogaard et al. 2013)	http://www.wofost.wur.nl
AquaCrop	V.6.0	(Foster et al. 2017)	http://www.fao.org/aquacrop/fr/

Benchmark of these models is available at Table 1.8. Except Aquacrop, all of them are using LAI as a proxy of biomass and use a Leaf area development model with a radiative component. Light isn't parameter of Aquacrop on the contrary of all these models. Aquacrop use

Table 1.8: Benchmarking of different Crop Growth models used in a winter wheat context (Palosuo et al. 2011)

	AquaCrop	APES	CROPSYST	DAISY	DSSAT	HERMES	FASSET	STICS	WOFOST
Leaf area development and light interception[a]	-	D	S	D	S	D	D	D	D
Light utilization[b]	-	RUE	RUE	P-R	RUE	RUE	P-R	RUE	P-R
Yield formationc	Y(HI,B)	Y(Prt)	Y(HI,B)	Y(Prt)	Yield(HI(Gn),B)	Y(HI,B)	Y(Prt)	Y(HI(Gn),B)	Y(Prt,B)
Crop phenology [d]	f(T)	f(T, DL, V)	f(T, DL, V)	f(T, DL, V)	f(T, DL, V)	f(T, DL)	f(T, DL, V)	f(T, DL, V)	f(T, DL)
Root distribution over depth [e]	EXP	EXP	LIN	EXP	EXP	EXP	EXP	SIG	LIN
Stresses involved [f]	W	W, N	W, N	W, N	W, N	W, N	W, N, A	W, N	W, N[j]
Water dynamics [g]	C	C	C	R	C	C	C	C	C[k]
Evapo-transpiration [h]	PM	P	PT	PM	PT	Makk	PM, TWj	P, PT or SW	P
Soil CN-model	CN	CN, P(3)	N, P(1)	CN, P(6), B	CN, P(4), B	CN, P(6), B	N, P(2)	C, P(3); B	-

[a] Leaf area development and light interception; Simple (=S) or Detailed (=D) approach.
[b] Light utilization or biomass growth: RUE = Simple (descriptive) Radiation use efficiency approach, P–R = Gross photosynthesis–respiration (for more details, see e.g. (Wien et al. 2010)).
[c] Y(x) yield formation depending on: HI = fixed harvest index, B = total (above-ground) biomass, Gn = number of grains, Prt = partitioning during reproductive stages.
[d] Crop phenology is a function (f) of: T = temperature, DL = photoperiod (day length), V = vernalisation; O = other water/nutrient stress effects considered.
[e] Root distribution over depth: linear (LIN), exponential (EXP), sigmoidal (SIG).
[f] Stresses involved: W = water stress, N = nitrogen stress, A = oxygen stress.
[g] Water dynamics approach: C = capacity approach, R = Richards approach.
[h] Method to calculate evapo-transpiration: P = Penman; PM = Penman–Monteith, PT = Priestley–Taylor, TW = Turc–Wendling, Makk = Makkink, HAR = Hargreaves, SW = Shuttleworth and Wallace (resistive model).
Soil CN model, N = N model, P(x) = x number of organic matter pools, B = microbial biomass pool.
[j] Nitrogen-limited yields can be calculated for given soil Nitrogen supply and N fertilizer applied.
[k] Only two soil layers (top- and subsoil) are distinguished.

a yield formation model based on a fixed harvest index and total biomass, while some models partition yield computation and harvest index computation. Crop phenology of aquacrop is independent from photoperiod while most of these include this parameter in computation. Water balance in most of models is based on capillarity approach, one model include richards equation, which is a computationally more expensive model. Evapotranspiration model seems to be a specificity of each model, soil parameters can include pools of organic mater, microbial biomass, while aquacrop mainly focus on run-off.

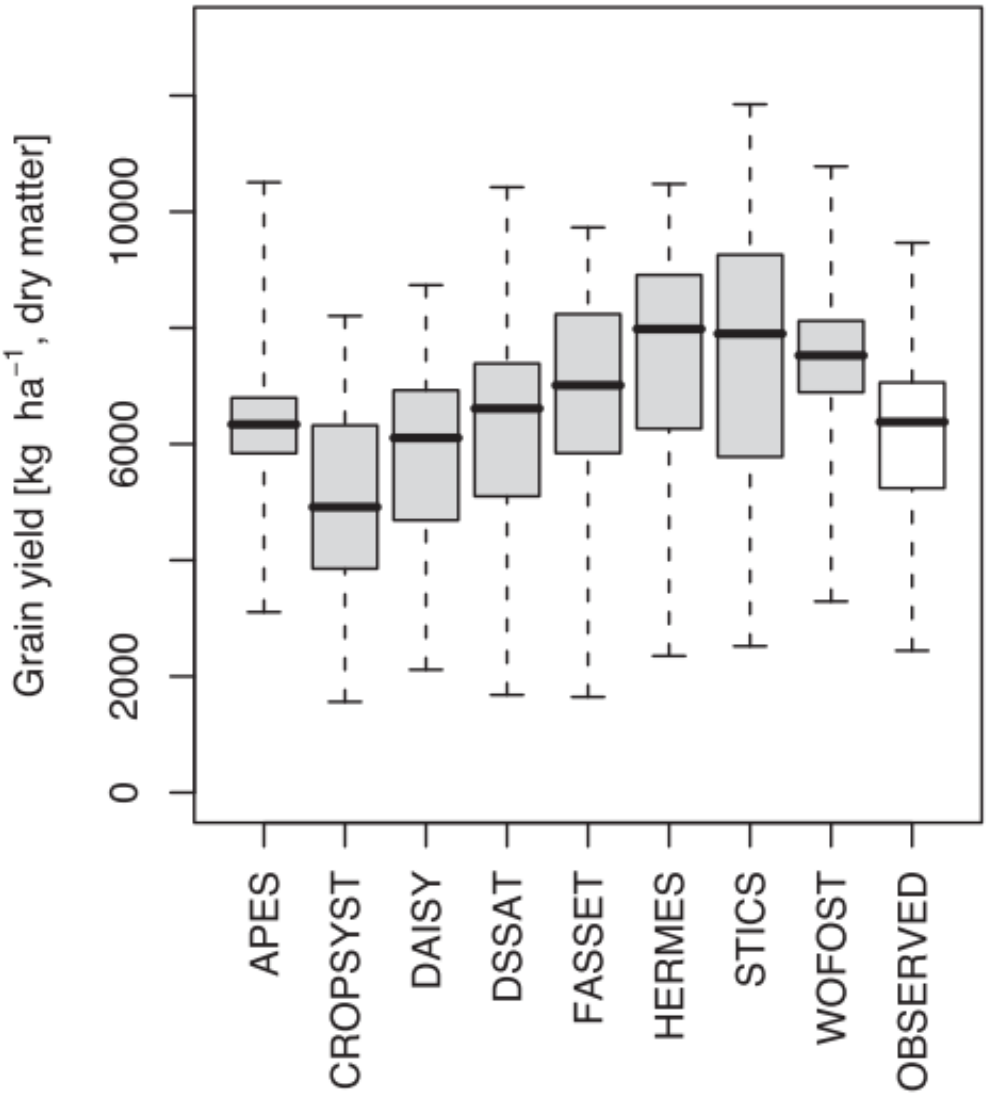

Figure 1.13: Prediction variation of existing Models

Figure 1.13 summarises the results of these different models, they generates a quite heterogeneous range of grain yield value. Most of the medians are significantly different of the real median, showing the intrinsic variability of crop growth models even using .

Chapter 2

Objectives & Research Questions

The primary purpose of this master thesis is to determine whether combining multispectral UAV and Sentinel 2 datasets may offer a more efficient way to analyze crops' growth compared to current satellite-based crop modeling approaches. The crop modeling environment used in this study is Aquacrop Model. The crop characteristics inputs of the model are partially derivated from satellite imagery, and a secondary objective is to determine if Aquacrop is adapted to high-resolution drone datasets.

Comparing crop growth models raises methodological issues; agronomists usually model crop growth modeling as a global process on the parcel. This study also aims to analyze growth curves locally using map displays of crop growth models. These comparisons require implementing a processing chain to retrieve crop growth models' parameters and their uncertainties.

The secondary objective of this work consists of studying the influence of spatial covariates on the winter wheat growth process. These covariables are related to topography, ploughing, and biochar patches located inside the parcel. The workflow followed is shown on Figure 2.1.

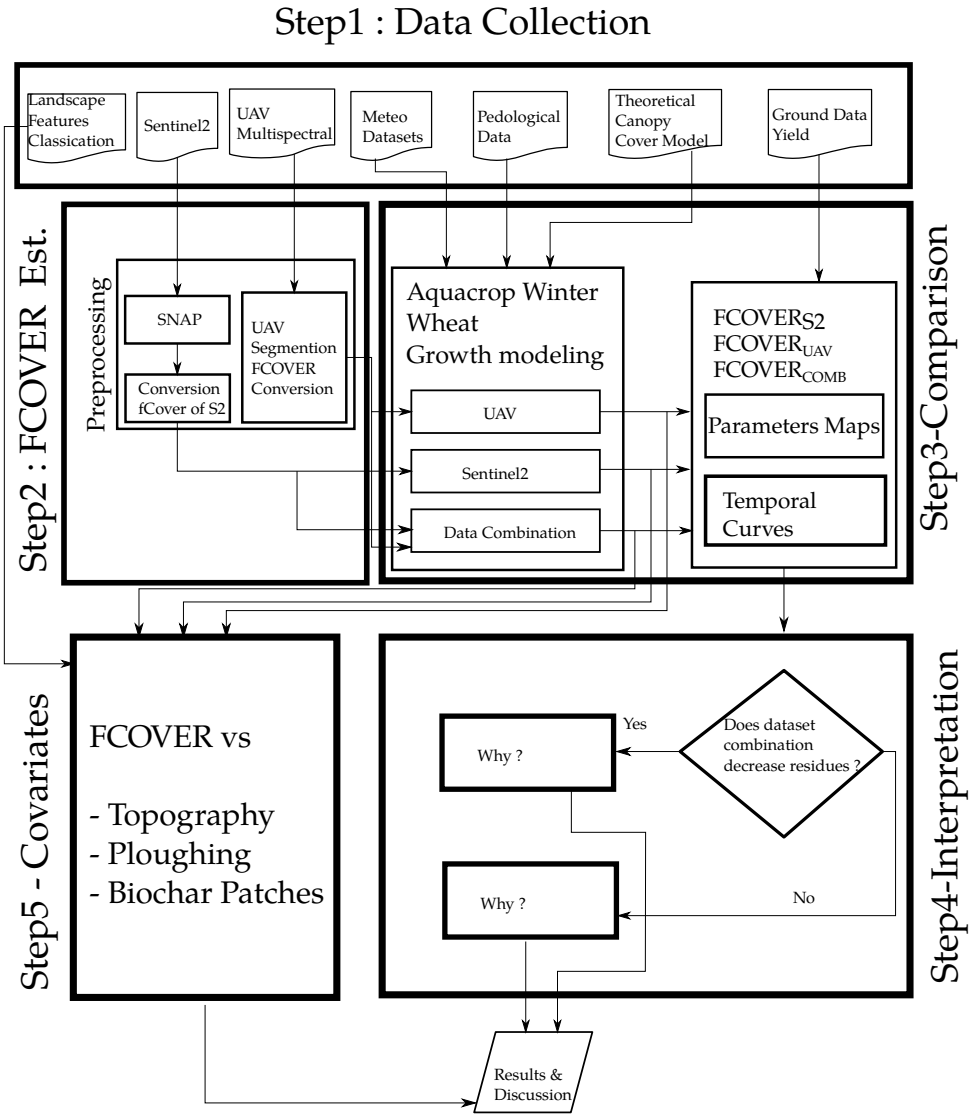

Figure 2.1: Workflow

Chapter 3

Material & Methods

3.1 Study area and climate

Figure 3.1: Map describing Study area

The experimental parcel is located in the Gembloux (province of Namur, Belgium), at

the coordinates (50° 31′ 14.5524″ N, 4° 44′ 56.0004″ E). This field surface is nearly$13\,\mathrm{ha}$ and biochar patches, caused by preindustrial charcoal kiln. The field is cultivated using conventional practices and a crop rotation by alternating beet, chicory, and winter wheat. According to (IRM 2019) Gembloux has a temperate oceanic climate, the annual average temperature in Gembloux is estimated around $9{,}6\,^{\circ}\mathrm{C}$ and annual precipation around $830\,\mathrm{mm}$.Parcel shows a convex profile with a maximum at its center, what is shown at Figure 3.2a. The soil type is a Luvisol characterized by a silt loam texture. According to (Legrain et al. 2011), soil typology summarised on Figure 3.2b is relatively homogeneous, imperfectly drained loamy soil, while some parts are moderately well drained in the northern and southern borders of the parcel. Borders are used as manoeuvring and storing areas, as they are located at the bottom of the slope, these soils are described as weakly gleyed.

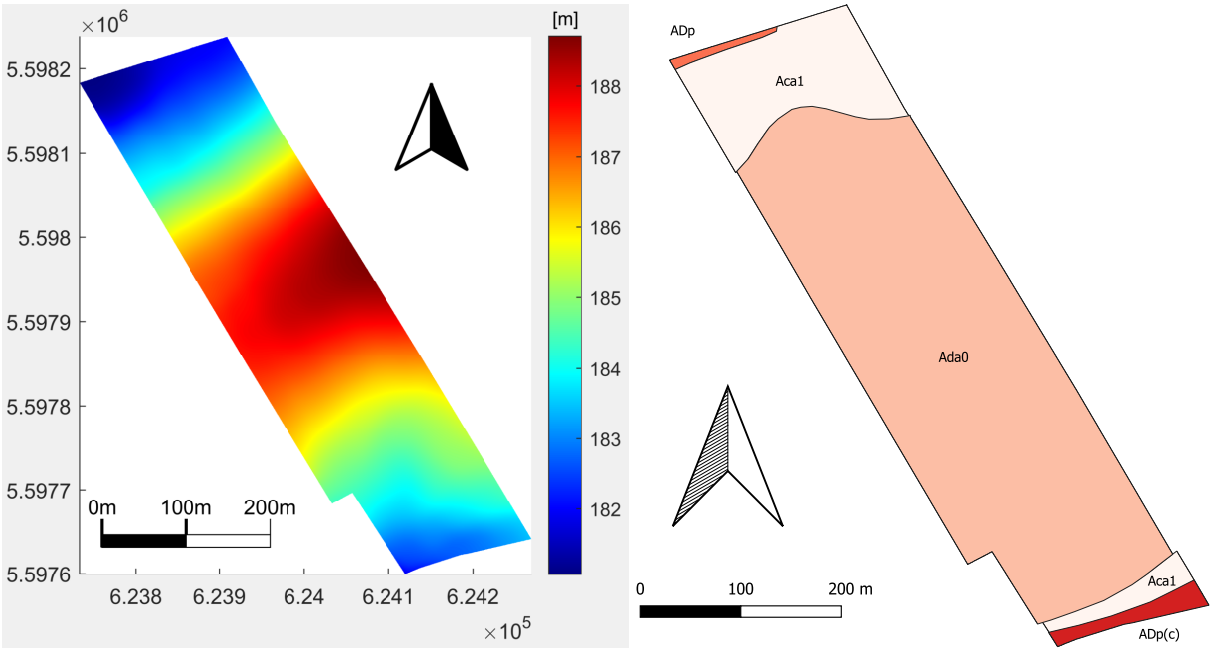

(a) (b)

Figure 3.2: Experimental Parcel - a)Topography of the field and b) Soil typology (Legrain et al. 2011)

Winter wheat was sowed the 6th of december 2018 and harvested the 18th of july 2019. In 2018, this field was first used to grow chicory and harvest took place at two different periods; a heatwave and a drought simultaneously occurs during summer 2018 (Vanhamel 2018). The Western [1] part was harvested in late September 2018, while the eastern part (late ploughing)

[1]The western (resp. eastern) is know as early (resp. late) ploughing in other parts of this document. These areas are also represented on Figure 3.1.

was collected at the end of November 2018, just before sowing. Ploughing date may influence soil properties depending on seasonal precipitation; when rain is over-abundant and depends on mechanical properties of soil, plow-pans occur, decreasing draining properties of soil and reducing root development (Bodson et al. 2011). Late sowing emergence tends also to be longer because of emergence, decreasing survival rate of young plants.

3.2 Software environment

Most of the implementations of this work are done using Matlab. `AquaCropOS_v60a` code, available at https://www.aquacropos.com was modifie to perform fast yield simulations. Additional toolbox used for this work are `export_fig`,`gmregress`,`GrTheory`,`plot2svg`, `stud-evapotransp` `subaxis` and `topotoolbox`. Code are available at https://github.com/lbataille/lbataille.github.io.git

3.3 UAV and Sentinel2 Datasets

The experimental set-up used ot collect multispectral UAV datasets is described by (Heidarian Dehkordi et al. 2020). The multispectral images were collected using a MicaSense RedEdge-M and downwelling light sensor, onboard a DJI Matrice 100 platform. The different bands, their wavelength range, and the S2 equivalent bands are summarised in Table 3.2.

(Heidarian Dehkordi et al. 2020). developed a postprocessing chain to construct a 3D representation of crops with of 3.7cm for hyperspectral images. Sentinel2 Images were collected on Copernicus, only dates providing a 5% or less cloud cover are selected. Figure 3.3 describes images availability during growing season.

Figure 3.3: Timeline - Datasets Availabilities

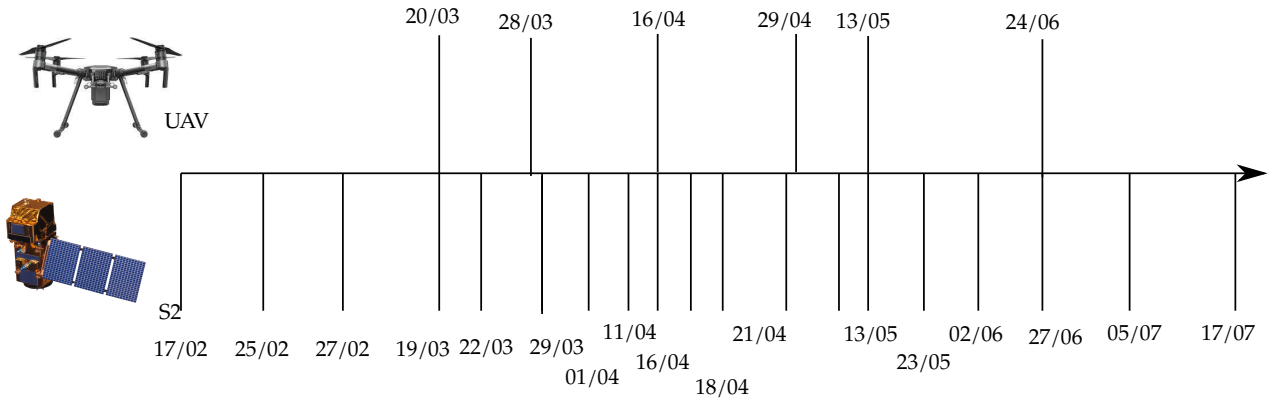

Table 3.1: Matlab script and function

filename	function
addNorth.m	Add a north pin on maps
applyMontecarlo.m	called by scriptMC to perform a Montecarlo Simulation
applyMontecarloClass.m	called by mcClass to perform Montecarlo Simulations and aggregate data by ploughing date or membership to biochar patches
applyMonteCarloFull.m	perform a Montecarlo on each pixel
calcHYPRES	Pedotransfer functions
calcIoc	compute Indicators of convergence
computeBBCHUPVT	Estimation of the phenology of crop
convertData2Grid	convert vector data to grid
convertReg2Grids	convert table of coeff to maps
corr2neigh	spatial correlation
day_length	compute day length
generateBoxplotFC	show errorbar diagram
generateDailyData	transcript Weather dataset to a daily dataset
getS2Images	find Sentinel2 images close to a date
plotTimeline	show phenological timeline
showResultsF	graphical features to build results of this master thesis

Table 3.2: UAV Spectral Bands and Sentinel2 Equivalent

Band Name	Wavelenght	Sentinel2 Equivalent
Red	668 ± 5	B04
Green	560 ± 10	B03
Blue	475 ± 10	B02
NIR	840 ± 20	B8/B8A
Red-Edge	717 ± 5	B05

3.4 FCOVER Estimators

Sentinel2 Processing

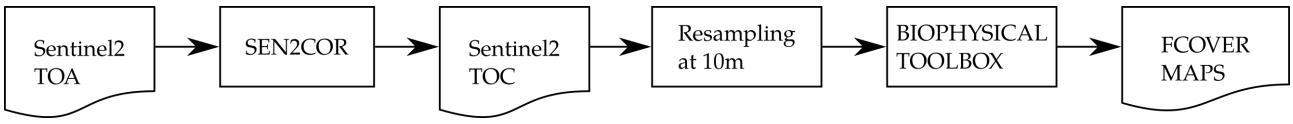

Figure 3.4: RGB components of Sentinel-2 Images and their corresponding FCOVER Maps

Sentinel2 images are processing on SNAP, a software edited by ESA dedicated to Satellite Image Processing. Processing steps are summarised on Figure 3.4. Raw Sentinel2 images represent top of the atmosphere reflectances (TOA) which may differ from top of canopy reflectance due to atmospheric conditions. A preprocessing toolbox based on SEN2COR apply atmospheric corrections to perform conversion. After a resampling procedure to get all the reflectance at a 10m resolution, a biophysical toolbox based on machine-learning satellite image retrieval method described in 1.4 converts TOC into FCOVER maps. Finally, sentinel2 Images are cropped to the study area using a R script. Example of these FCOVER maps are shown at Figure 3.5.

UAV - Segmentation and FCOVER Inference

UAV images are processed using a uniform threshold established by (Heidarian Dehkordi et al. 2020), segmentation process is described by (3.1). R,G,B are the digitial number describing red, green and blue reflectances.

$$[(G - B) > \alpha \text{ and } [(G - R) > \beta] \text{ where } \alpha = \beta = 20 \tag{3.1}$$

This segmentation allows to transcript multispectral reflectance images into masks. A zoom on mask is shown on Figure 3.7. FCOVER is computed by measuring the proportion of Segmentation pixels inside a grid of given width and height. Two grid resolution are tested a 10m grid which corresponds to Sentinel2 images pixels and a 2m square grid.

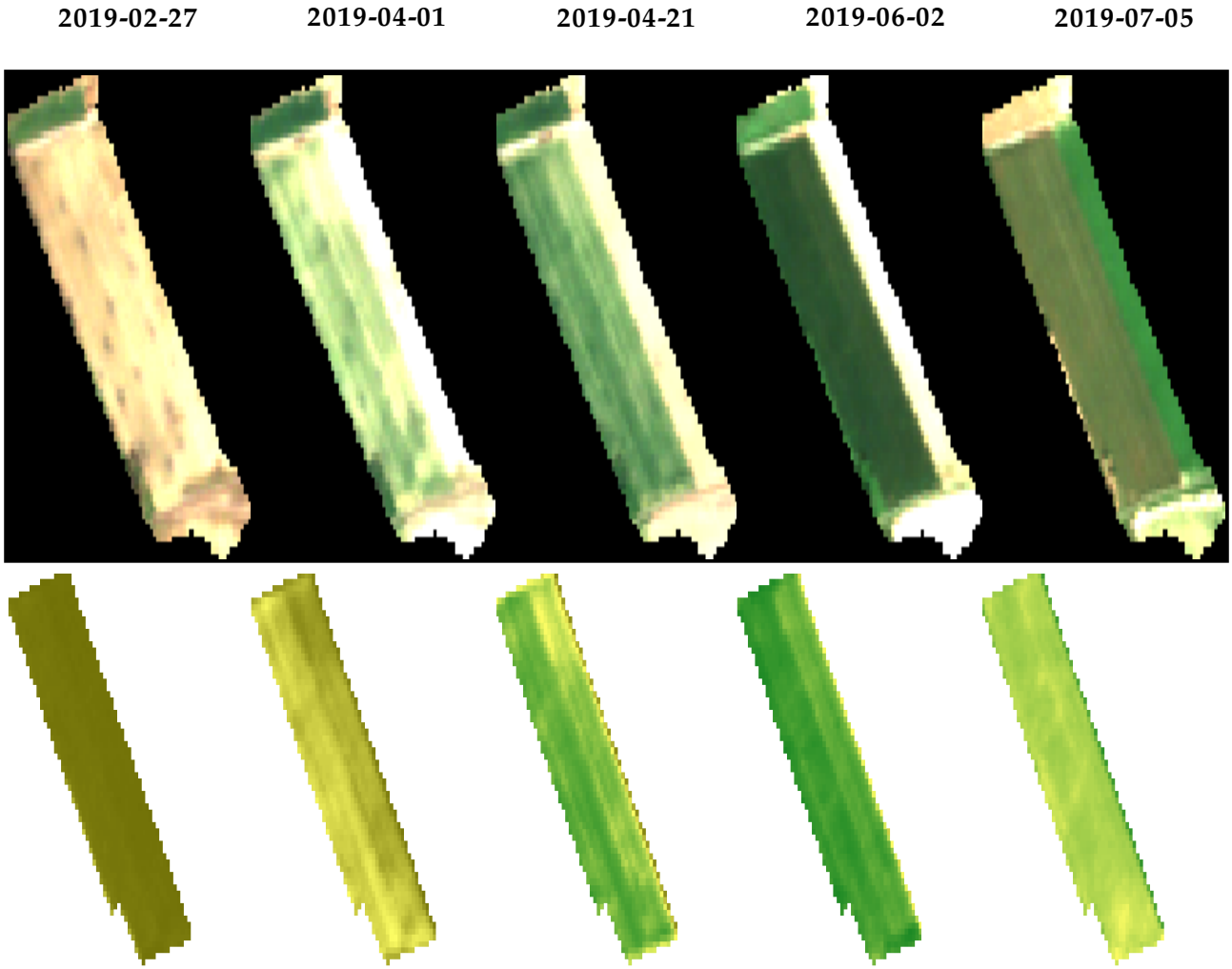

Figure 3.5: RGB components of Sentinel-2 Images and their corresponding FCOVER Maps

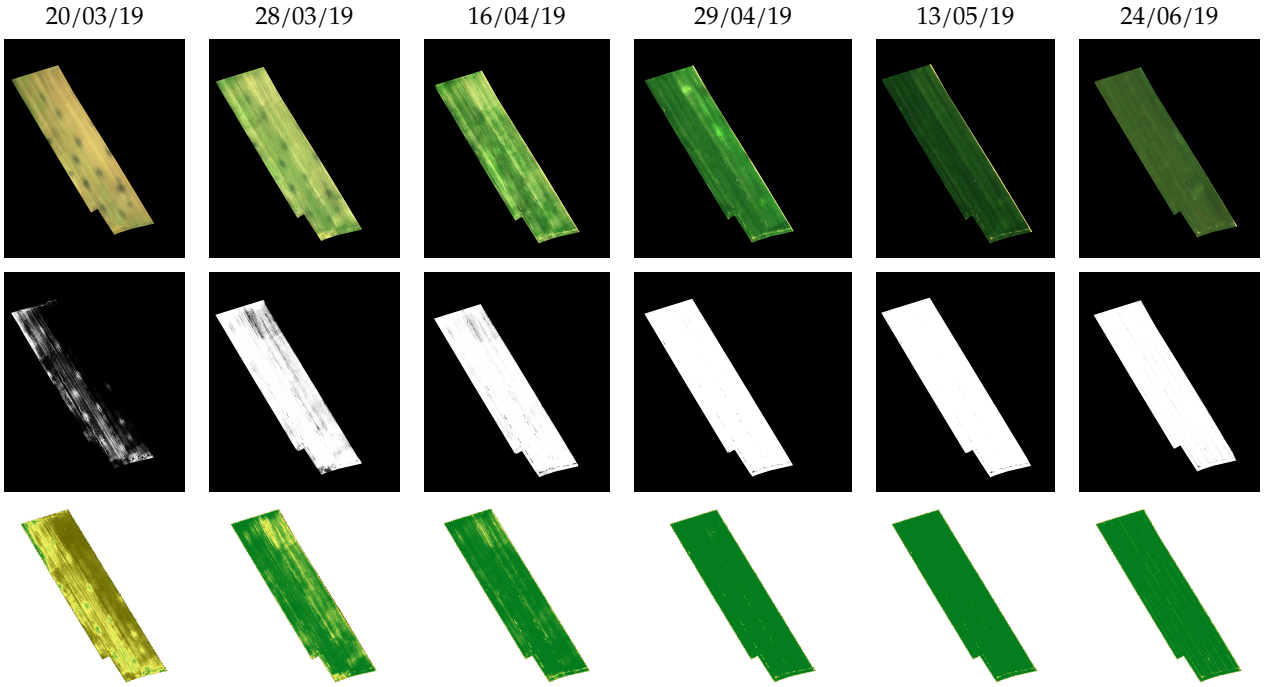

Figure 3.6: RGB, Masks and FCOVER (2m grid aggregation) at the parcle scale

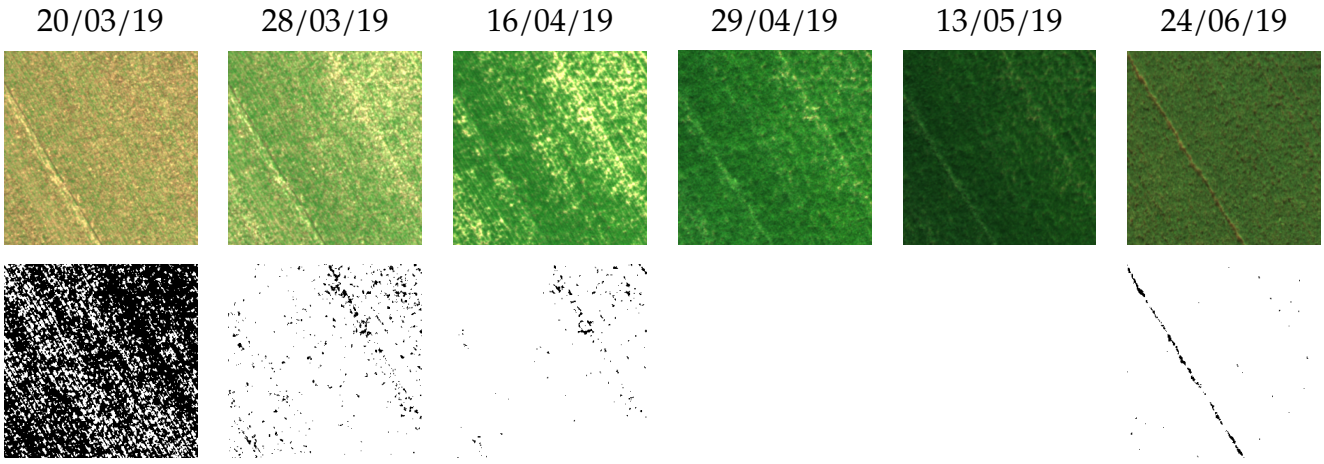

Figure 3.7: Zoom a 10m x 10m square and segmented pixels corresponding to this area

3.5 FCOVER Model - Regression Method

Aquacrop is based on a FCOVER model presented in section **??** by (1.26) , (1.27), (1.28), (1.29),1.30) and (1.31). This kind of model defined by a piecewise non-linear equation requires to implement a regression, which is presented on Figure 3.8.

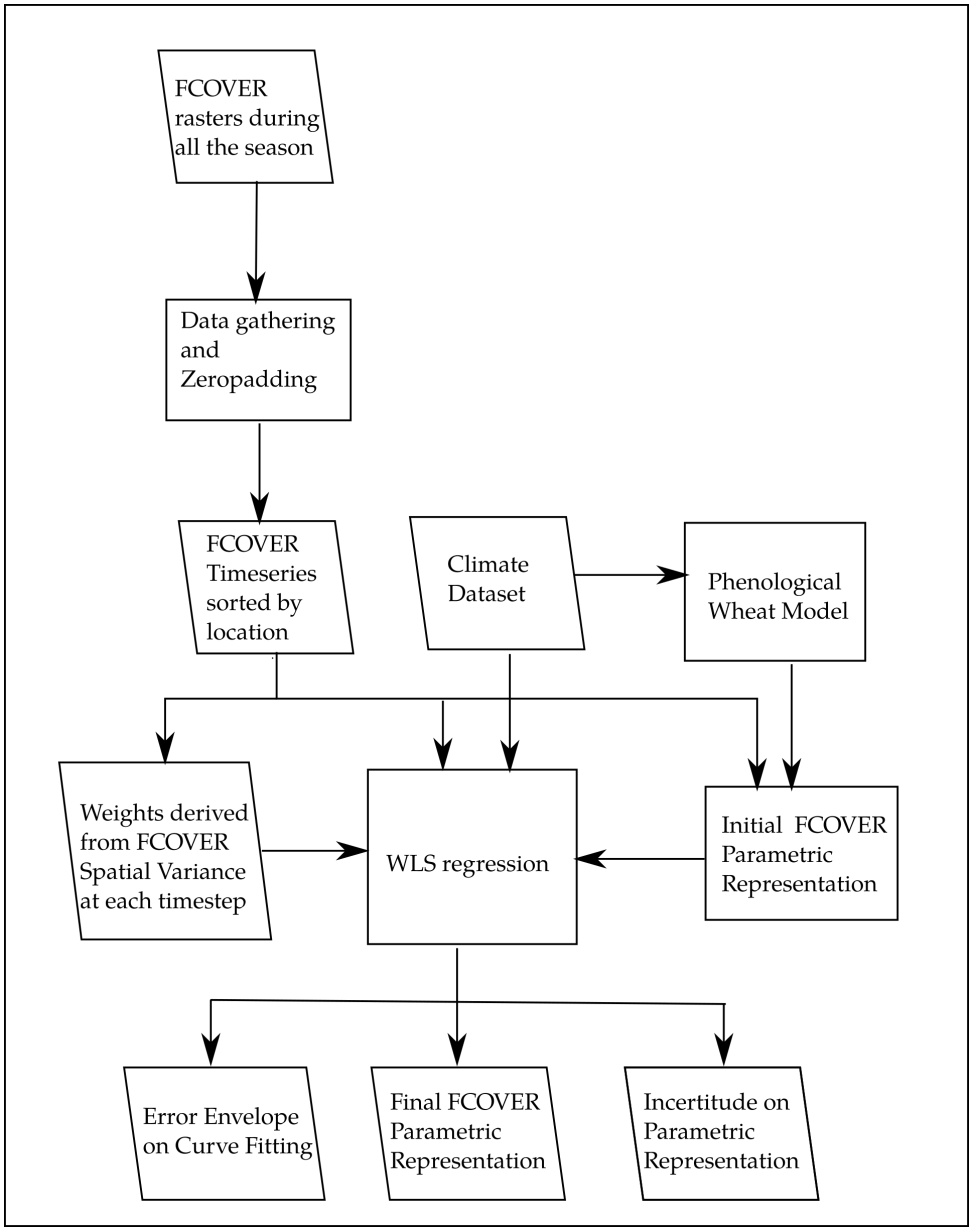

Figure 3.8: FCOVER Regression - Block-diagram representation

Data Preprocessing & Zero Padding

Preprocessing steps are described on Figure 3.9. Information of multiple rasters is gathered in a table sorted by position and by date. Zero padding is applied to artificially impose a zero value long time before emergence and long after senescence. A phenology model described by Appendix A.2 is used to make assumptions on emergence date. Total Senescence is assumed after crop harvest.

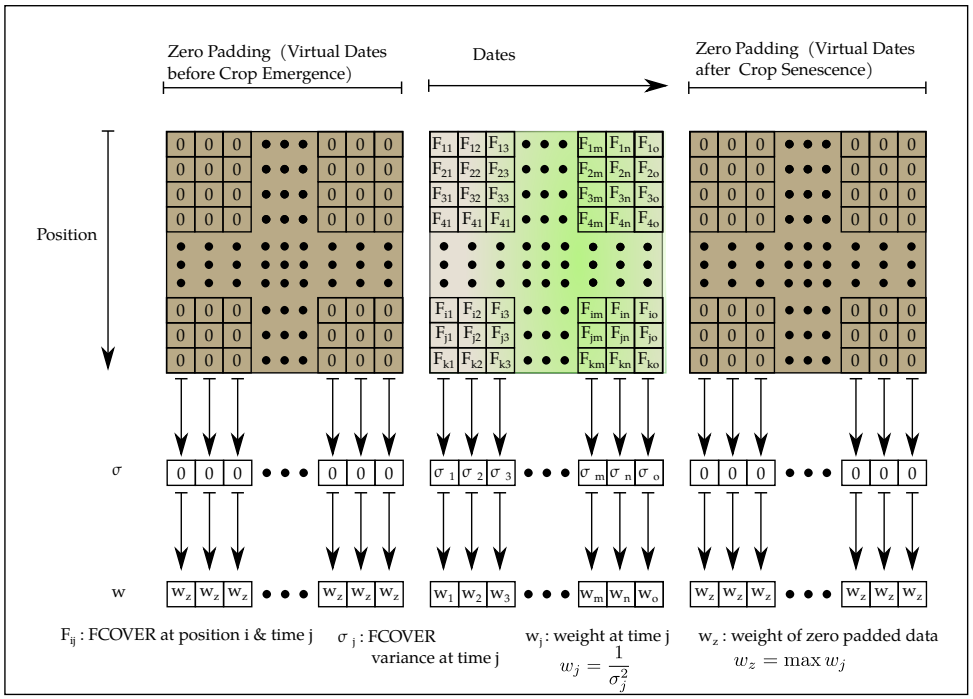

Figure 3.9: FCOVER Regression - Block-diagram representation

FCOVER - Initial Estimation of Growth Curve Parameters

Initialisation is described on Figure 3.10. First step consists in interpolation data and detecting GDDc_{50}, a linear regression is applied selecting datas around this value to determine CGC. These values are used to compute CC_0. Maximal value is initialized as the 95$^{\text{th}}$ percentile of FCOVER. GDDc_{Sen} is initialized as the moment at which curve decreases under 90% of estimated CC_x.

FCOVER - WLS Method - Iterative Process

The computation of the growth curve parameters relies on a weighted least squares (WLS) estimator. Uncertainties are considered using variance of complete parcel at each date, to

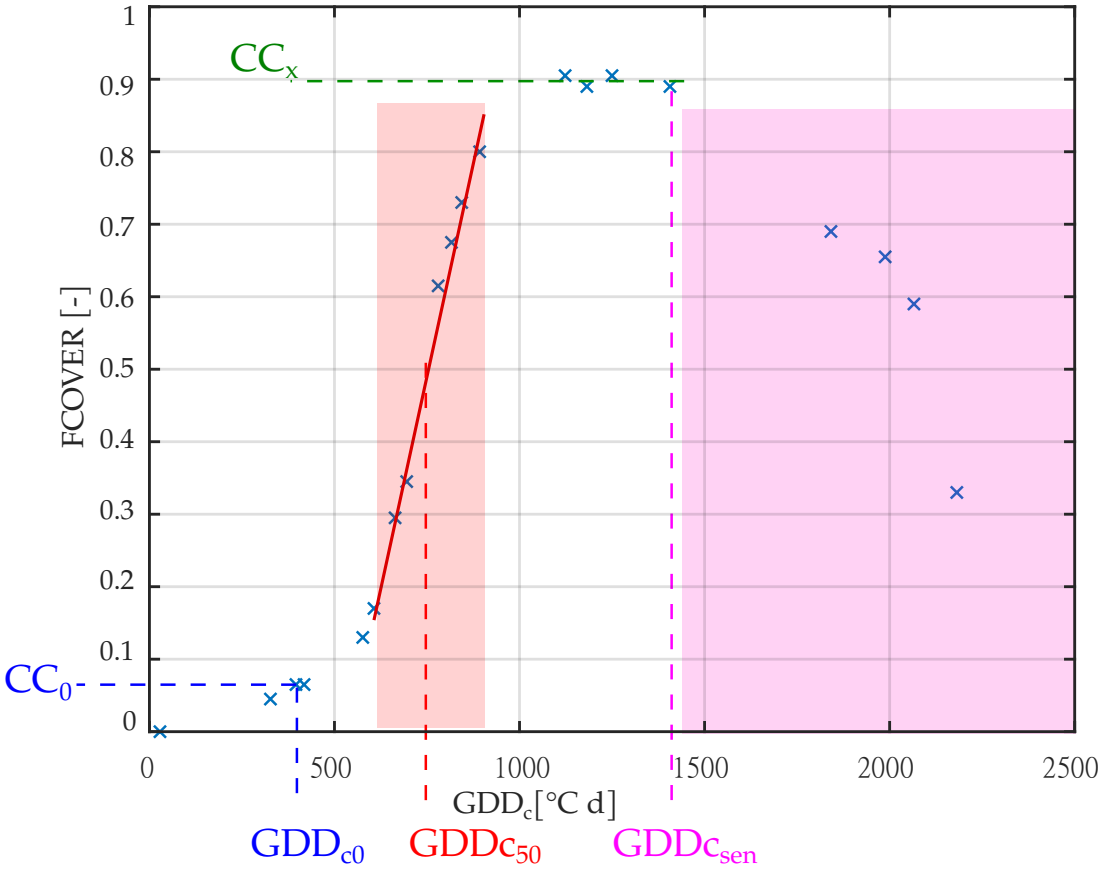

$$FCOVER_{50} \sim CGC\ (GDDc\ -\ GDDc_{50}) + 0.5$$

$$CC_0 \sim 0.5\ CC_x\ e^{-(GDD_{c50}-GDDc0)\ CGC}$$

$$CC_{sen} \sim CC_x\ \{1-0.05\ [\ e^{3.33\ CDC\ (GDDc\ -GDDcsen)/(CCx+2.29)}-1]\}$$

(a)

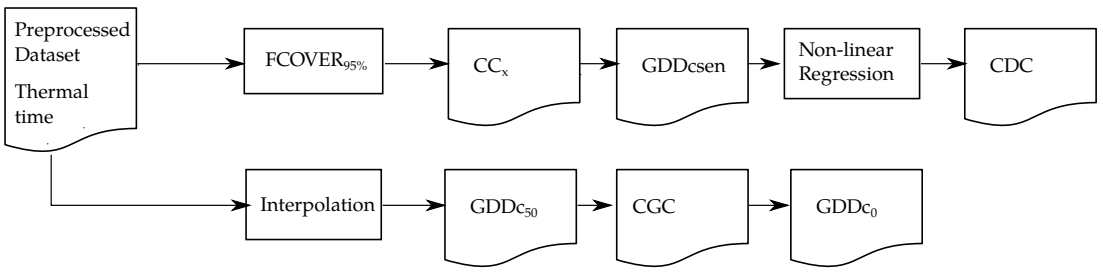

(b)

Figure 3.10: Initialisation of FCOVER Model Parameters - a) Graphical representation of methodology and b) Flow chart describing initialization of Growth Curve paremeters

prevent the influence of outlier on regression.

$$\begin{cases} \mu_j = \sum_{i=1}^{\text{NPoints}} \dfrac{\text{FCOVER}_{ij}}{\text{NPoints}} & (3.2) \\ \sigma_j^2 = \sum_{i=1}^{\text{NPoints}} \dfrac{(\text{FCOVER}_{ij} - \mu_j)^2}{\text{NPoints} - 1} & (3.3) \\ w_j = \dfrac{1}{\sigma_j^2} \text{ and } w_j = \max w_j \text{ for all zero padded data} & (3.4) \end{cases}$$

μ_j describes the average of complete parcel at a date j and σ_j^2. FCOVER_{ij} describes the Fractional Vegetation cover at a point i at a date j. Zero padded data have a zero variance, they are assign the weight w_{max}, the highest weight of non-padded datas. Optimisation problem is expressed by an objective function (3.5)) subjected to constraints (3.6) ,(3.7), (3.8), (3.9), (3.10), (3.11) and (3.12). $\text{GDDc}^\star_{50\%}$,$\text{GDDc}^\star_{Sen}$,$\text{CC}^\star_0$,$\text{CC}^\star_x$,$\text{CGC}^\star$, $\text{CDC}^\star$ are the initial estimation of fitting parameters established at subsection 3.5.

$$\min_{\overrightarrow{\zeta}} \left[\sum_{j=1}^{\text{NDates}} w_j (\text{FCOVER}_{ij} - \text{FCOVER}(\text{GDDc}_j, \overrightarrow{\zeta}))^2 \right] \quad (3.5)$$

$$\text{where } \overrightarrow{\zeta} = (\text{GDDc}_0, \text{GDDc}_{Sen}, \text{CC}_0, \text{CC}_x, \text{CGC}, \text{CDC})$$

subject to

$$\begin{cases} \text{GDDc}_0 < 0.5\,\text{GDDc}^\star_{50} & (3.6) \\ \text{GDDc}_{sen} \geq \text{GDDc}^\star_{sen} \text{ and } \text{GDDc}_{sen} < 1.5\,\text{GDDc}^\star_{sen} & (3.7) \\ \text{CC}_0 \leq 0.25\,\text{CC}^\star_x & (3.8) \\ \text{CC}_x \leq 1 \text{ and } \text{CC}_x \geq \text{CC}^\star_x & (3.9) \\ \text{CGC} > 0.25\,\text{CGC}^\star \text{ and } \text{CGC} \leq 3\,\text{CGC}^\star & (3.10) \\ \text{CDC} > 0.005\,\text{CGC}^\star \text{ and } \text{CDC} \leq 2\,\text{CDC}^\star & (3.11) \\ \text{GDDc}_0, \text{GDDc}_{Sen}, \text{CC}_0, \text{CC}_x, \text{CGC}, \text{CDC} > 0 & (3.12) \end{cases}$$

A Levenberg-Marquardt algorithm is used to solve this optimisation problem on Matlab. Variation range of parameter is selected to prevent convergence towards a non-physiological minimum, while keeping enough flexibility and avoiding convergence to a local minimum related caused by a too restrictive constraint choice.

3.6 Yield - Aquacrop Simulations

AquacropOS is a Matlab version of Aquacrop, which is available at https://www.aquacropos.com. Source codes modifications allows to efficiently incorporate FCOVER model parameters fitted from time series. Winter Wheat growing characteristics unrelated to FCOVER arise from

a KULeuven dataset, which was used to perform crop modelling under climate change (Vanuytrecht, Raes, and Willems 2016). Weather data were collected during the whole growing season, they are summarised in Appendix A.4 and soil textural fractions allows to compute hydropedological parameters, using a pedotransfer function. Pedotransfer model is HYPRES, a model dedicated to European soils (Wösten et al. 1999), hydrological properties are assumed uniform on the parcel. Weather datasets are converted to provide daily datasets, daily reference evapotranspiration ET_0 is computed using Penman-Monteith Equation (Allen et al. 1998). G is neglected during the period.

$$\mathrm{ET}_0 = \frac{0.408\Delta\left(R_n - G\right) + \gamma\frac{900}{T_{air}+273}u_2\left(e_s - e_a\right)}{\Delta + \gamma\left(1 + 0.34u_2\right)} \tag{3.13}$$

- ET_0 reference evapotranspiration $[\mathrm{mm\,d^{-1}}]$,
- R_n net radiation at the crop surface $[\mathrm{MJm^{-2}d^{-1}}]$,
- G soil heat flux density $[\mathrm{MJm^{-2}d^{-1}}]$,
- T_{air} temperature at 2 m height $[\mathrm{°C}]$,
- u_2 wind speed at 2 m height $[\mathrm{m\,s^{-1}}]$,
- e_s saturation vapour pressure $[\mathrm{kPa}]$,
- e_a actual vapour pressure $[\mathrm{kPa}]$,
- $e_s - e_a$ saturation vapour pressure deficit $[\mathrm{kPa}]$,
- Δ slope vapour pressure curve $[\mathrm{kPa°C^{-1}}]$,
- γ psychrometric constant $[\mathrm{kPa°C^{-1}}]$.

3.7 Uncertainties evaluation

Uncertainties are estimated using a Montecarlo method, objective is to determine which parts of the growing curves are the most subject to uncertainties. The variation range is fixed thanks to the extremal values at teach date. A function applying Montecarlo to generate an uncertainties map towards growing curve parameters. The number of repetitions used to generate statistics on model predictions is fixed to 150.

3.8 Covariates

Different covariates have been studied during this work to determine their influence on FCOVER. Most of them are topographic variables, derived from a DEM layer downloaded from (NASA 2021). Topography of the parcel is studied using a SRTM elevation map, allowing to compute different topographical variables including slope, plane curvature, profile curvature, tangential curvature, the deviation of the orientation of the slope towards the North (SDevtN) and Total Wetness Index (TWI). These values are computed using SAGAGIS processing tools available on QGIS. Formulae (3.14) and (3.15) defines respectively TWI and SDevtN.

$$\mathrm{TWI} = \ln \frac{\mathrm{Acc}}{\tan S_R} \text{ where } S_R \text{ is the slope given in radians} \tag{3.14}$$

$$\mathrm{SDevtN} = \min(\mathrm{Aspect}, 360 - \mathrm{Aspect}) \tag{3.15}$$

All these covariates are shown on Figure1.4 in Appendix A.7. Other covariates are generated by digitalizing ploughing areas (contours of the early and late ploughing are shown on Figure 3.2a and biochar patches digitalization is illustrated at Figure 3.11.

This vector shape is vectorized using raster resolution. A pixel is considered a member of a biochar patch when its surface is located at 60 % inside the patch.

Figure 3.11: Biochar patches digitalization

Chapter 4

Results & Discussion

4.1 FCOVER Estimation and Yields - Comparison of S2 and UAV

FCOVER Models - Comparison of the results

As described in Table 1.6, the growth curves are related to six distinct parameters. Figure 4.1a describes models generated using different different FCOVER-time-series. Predictions performed from only UAV tend to grow earlier, faster and to a higher maximal FCOVER than sentinel2.

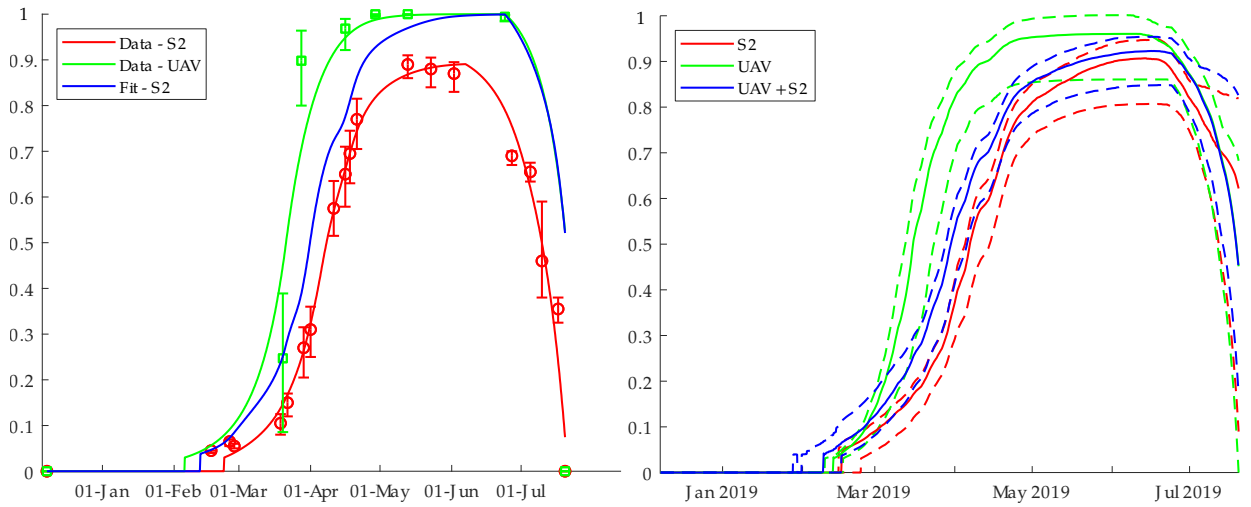

Figure 4.1: Comparison of global data - Comparison between Sentinel 2 FCOVER Maps and UAV raw data - a) Complete parcel and b) Uncertainties

The senescence process is poorly described by UAV dataset; FCOVER decreasing is caused by the assumption that the FCOVER value is zero after the harvest. Figure 4.1b is generated using a Montecarlo process, and the variation range is fixed by spatial variation of the parcel. Uncertainties look higher on the UAV dataset; indeed experimental dataset reaches a maximal plate so fast that model encounters difficulties to describe decay growing phase properly. The maximal uncertainties is noticed at the beginning of the decline phase, and it corresponds to a period at which data points are scarcer in each category, while the ecosystem changing rate is high. Data combination provides intermediate results, higher maximal FCOVER than Sentinel2 but decease phase is better-described thanks to Sentinel2 dataset.

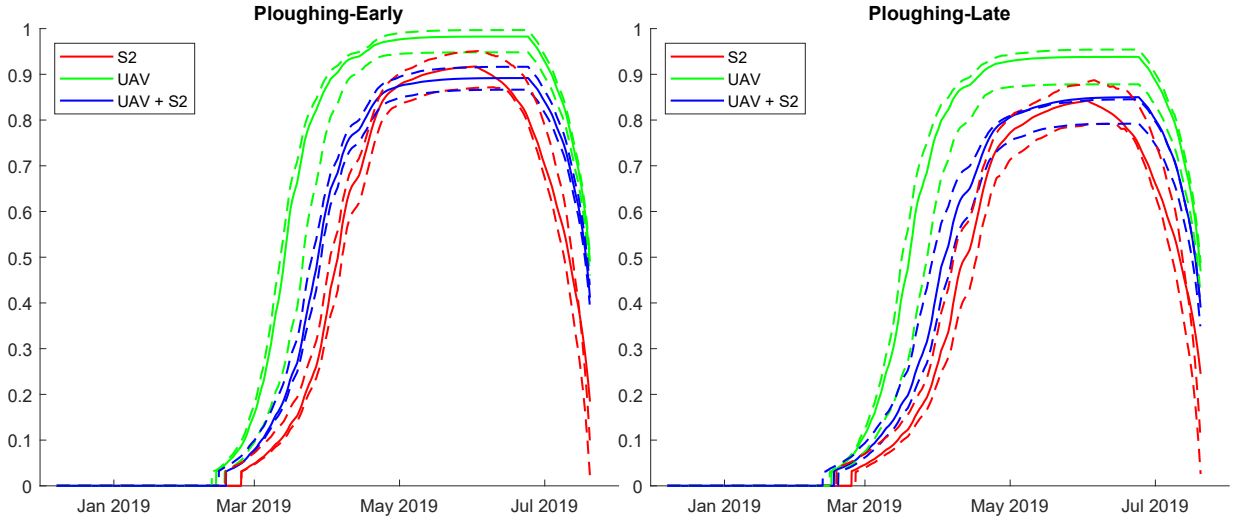

Figure 4.2: Comparison of global data - Early Ploughing vs Late Poughing - Comparison between Sentinel 2 FCOVER Maps and UAV raw data - a) Complete parcel and b) Uncertainties

The equivalent Montecarlo Method is applied to compare biochar patches to the rest of the parcel and detect potential differences between early plowed and late plowed areas during the growing process. Biochar patches don't show an apparent graphical difference with the rest of the parcel, while slight differences are visible on Figure 4.2. The late Ploughing curve tends to start a bit later, and the growth rate is lower than early plowing where curve usually reaches higher levels.

Models comparison - Maps

Comparison are performed if important differences are observed. Maps of CC_0, CDC and GDD_{sen} are shown in Appendix. Figure 4.3 describes the thermal time at which 90% of emergence occurs; it confirms previously detected trends, FCOVER models generated from UAV

suggest an earlier emergence than Sentinel2. Peaks are noticed on the UAV FCOVER map around some of the south-facing parts of the field, suggesting that biochar darker soils absorb sun radiations more efficiently and allow an earlier vegetation development. Sentinel2 images suggest that later plowed half of the field develop a bit later.

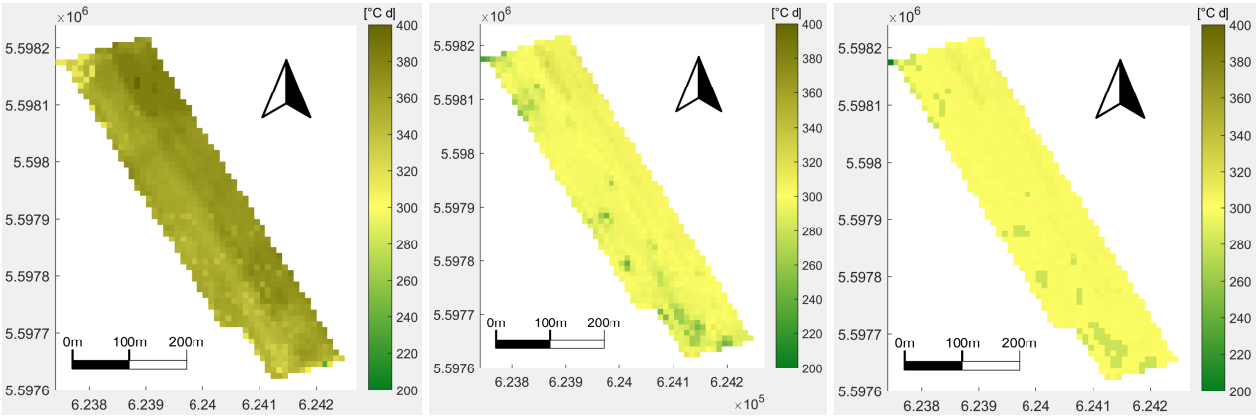

(a) (b) (c)

Figure 4.3: $GDDc_0$ - Thermal time at 90% of emergence - 10 m - a) Sentinel2, b) UAV and c) S2+UAV

CGC descibes the maximal growth rate of crops. As FCOVER curves generated from UAV images are always higher than Sentinel2 models, this trends is confirmed by the ranges of values observed on Figure **??**. UAV map suggests that growth curve is a bit steeper on biochar spots located in the the southern part of the parcel. All the scenarios noticed an area in the northern part of the parcel where growing rate is lower. This trend is confirmed by Figure 3.6 and 3.5.

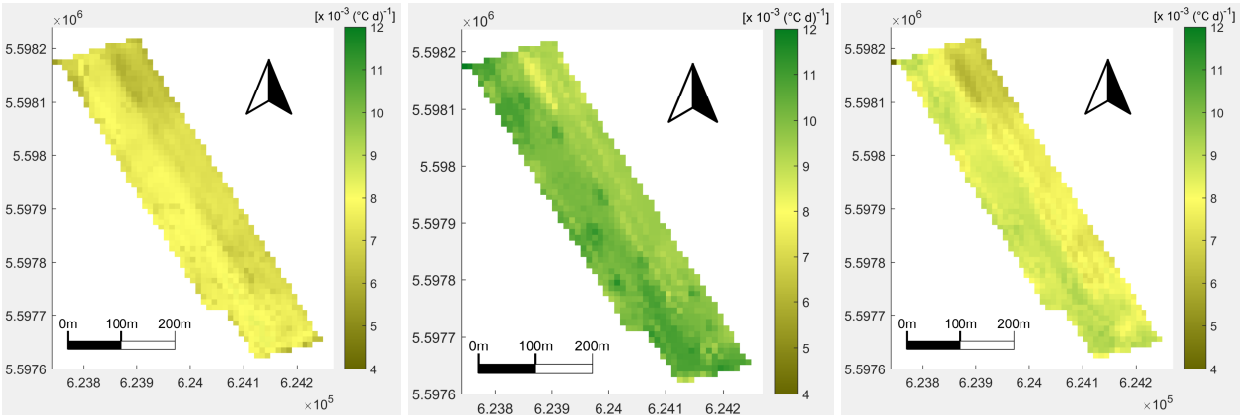

(a) (b) (c)

Figure 4.4: CGC - 10 m - a) Sentinel2, b) UAV and c) S2+UAV

Finally, another preponderant variable describing crop growth processes is the maximal canopy cover. This variable is uniform in UAV images, while a big difference is noted between early and late plowed parts of the field in the case of Sentinel2 Images.

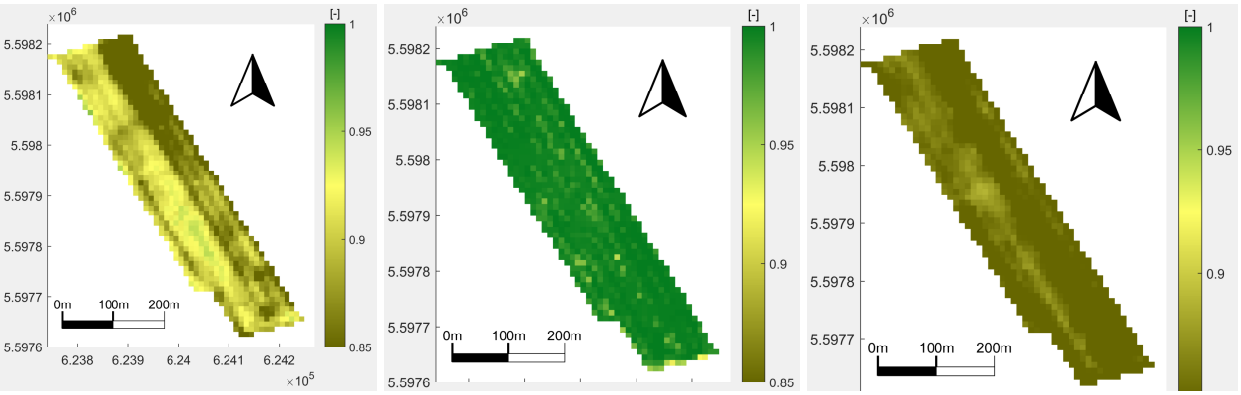

(a) (b) (c)

Figure 4.5: CC_x - 10 m - a) Sentinel2, b) UAV and c) S2+UAV

Yield generated by Aquacrop simulations can summarise crop growth models results. Figure 4.6 describes spatial distribution of yield. Figure 4.6d was computed by (Heidarian Dehkordi et al. 2020) using a semi-empiric model based on sCCCI defined in Table 1.4. This reference map has no similarity with modeled yields. Comparing ranges tends to show that Aquacrop strongly overestimates yield in the case of the UAV dataset. In contrast, Sentinel2 leads to an underestimation. Data combination provides an intermediate value closer to the semi-empirical map.

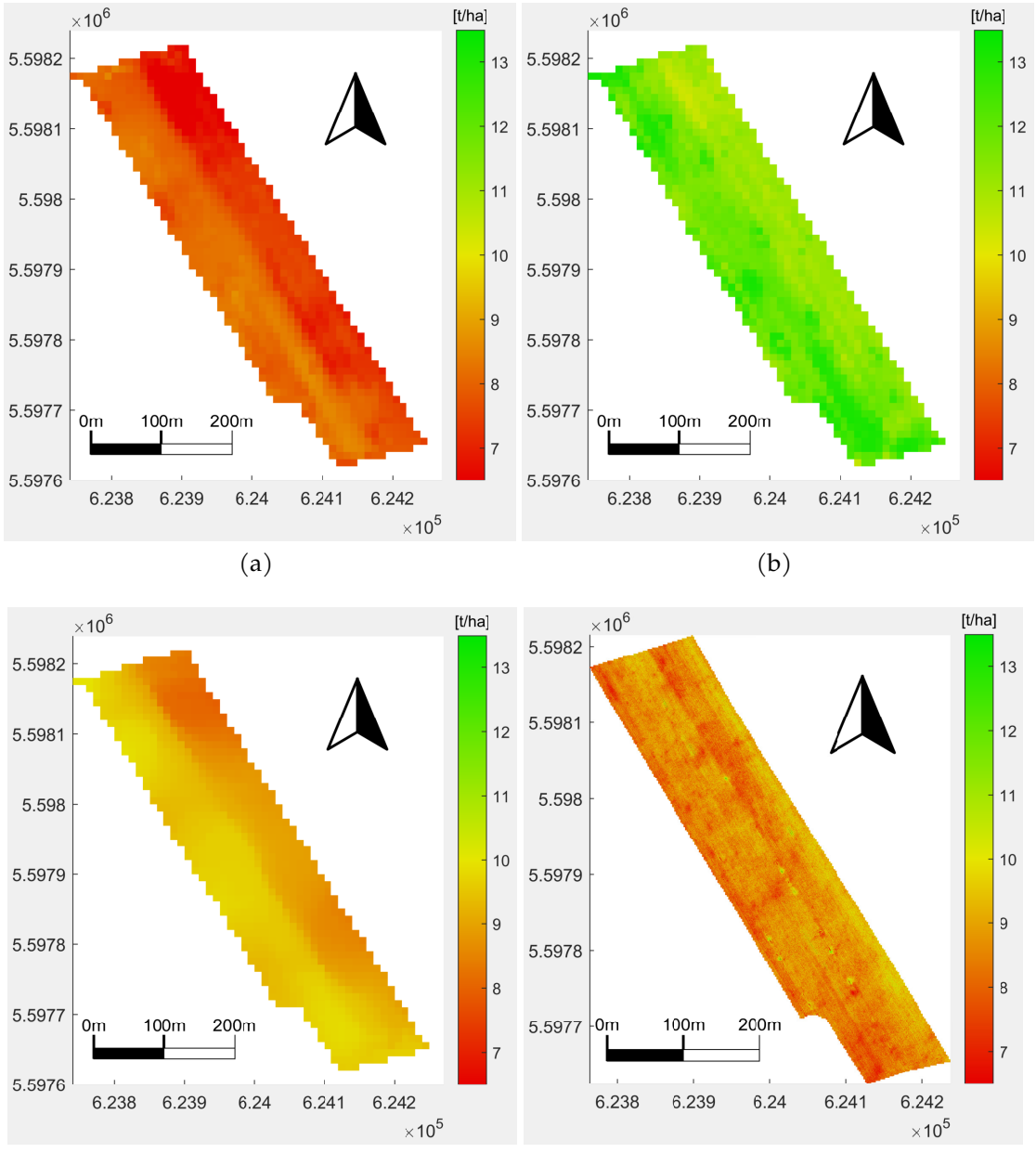

Figure 4.6: Yield prediction maps - 10 m - a) Sentinel2, b) UAV, c) S2+UAV and d) ML - sCCCI

4.2 Model Comparison - Correlation plot

Previous figures showed comparisons to detect a potential spatial patter Figure 4.7describes relations between the different models. Range of the parameters are similar, correlation between UAV and Sentinel2 estimations are weak and relative bias are non-negligible.

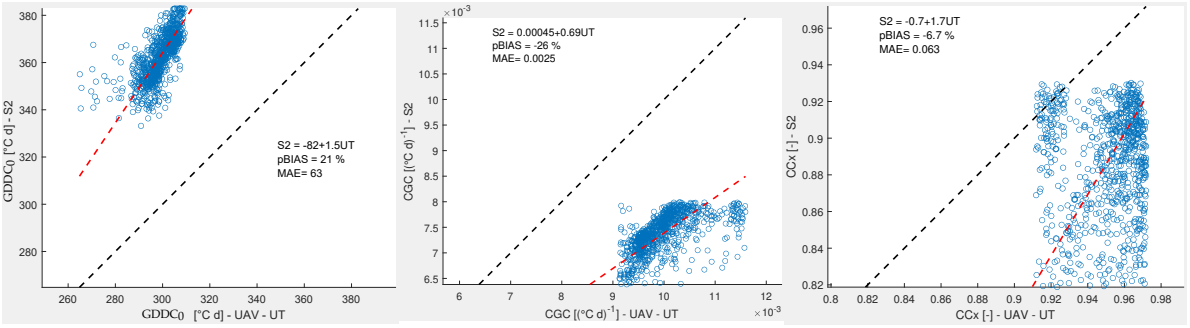

(a) $GDDc_0$ - S2 - UT (b) CGC- S2 - UT (c) CCx-S2 - UT

Figure 4.7: Model comparison Sentinel2 vs UAV - $GDDc_0$, CGC and CCx

The situation is quite similar for the yields, datasets are weakly correlated, UAV and Sentinel2 estimations shows a strong difference around 4t/ha. UAV Yields are very high compared to reference values shown on Figure 4.8d (Palosuo et al. 2011; Vanuytrecht, Raes, and Willems 2016). These high value are the consequence of ohter crop characteristic data, which are partially derivated from remote-sensing retrieval methods.

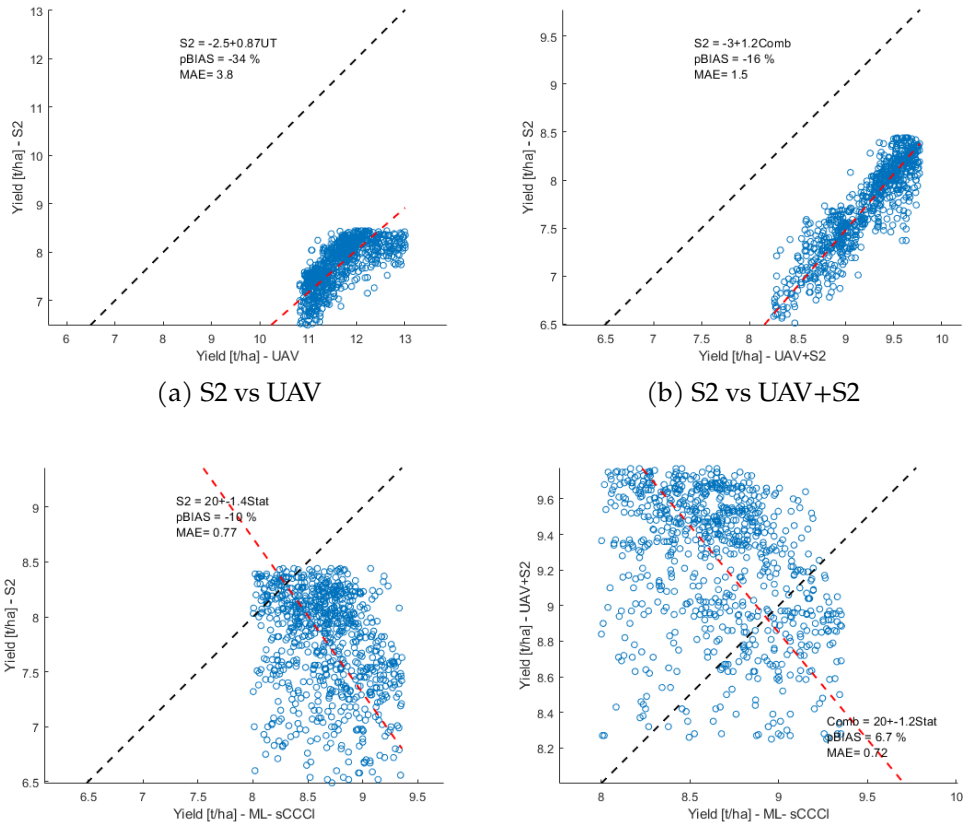

(a) S2 vs UAV

(b) S2 vs UAV+S2

(c) S2 vs ML

(d) UAV + S2 - ML

Figure 4.8: Yield Comparison

4.3 Interpretation according to different covariates

Categorial Variables - Kilns and Ploughing Influence

Amongst tested covariates, categorical covariables, describing the biochar patches influence and the ploughing, tends to have a high on the crop growth process variables. COB describes Centuries old biochar soil, while Ref describes soils of the parcel which isn't part of a biochar patche. Early and late describes the ploughing date. These variables are described on Figures 4.9, 4.10, 4.11 and 4.12. Stastistical tests are performed at two level; a first test is used to study similarity betweens medians of different datasets on similar parts of the field while second one compares medians of different field parts for the same dataset.

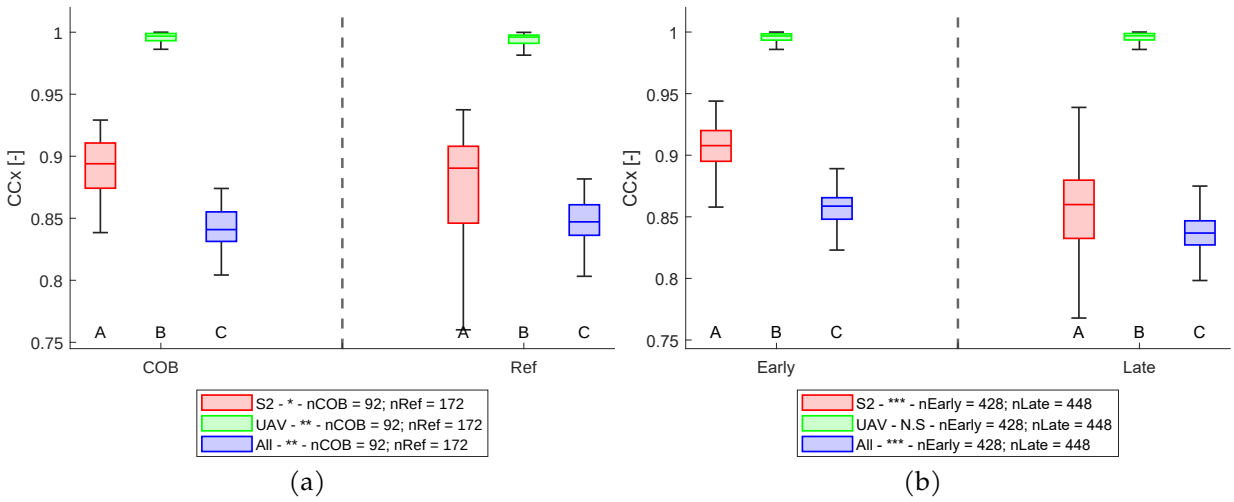

(a) (b)

Figure 4.9: CC_x - 10 m - FCOVER maximal value - categorical covariate influences - a) Biochar Patches and b) Ploughing

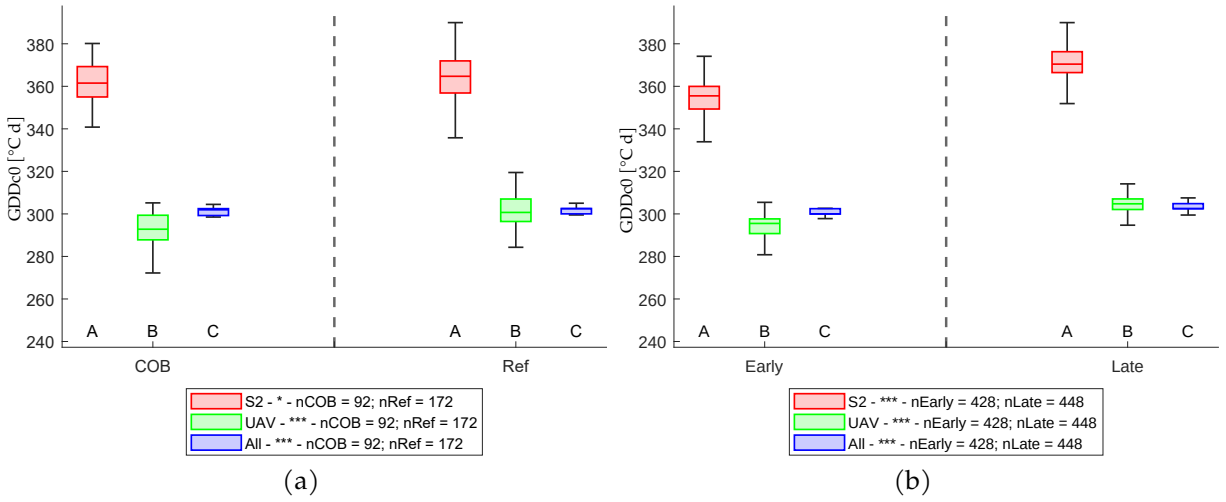

(a) (b)

Figure 4.10: GDDc_0 - 10 m - Thermal time required for emergence - categorical covariate influences - a) Biochar Patches and b) Ploughing

Sentinel2 images detects less dissimilarity between COB and Ref than other methods, test aren't significatively different for CGC, yield and significant in the case of CC_x. In the other situations, datasets tends to vary extremely significantly on each each factor, trends suggests that an earlier and faster growth and a higher yield are encountered in around biochar patches and on the half ploughed in September.

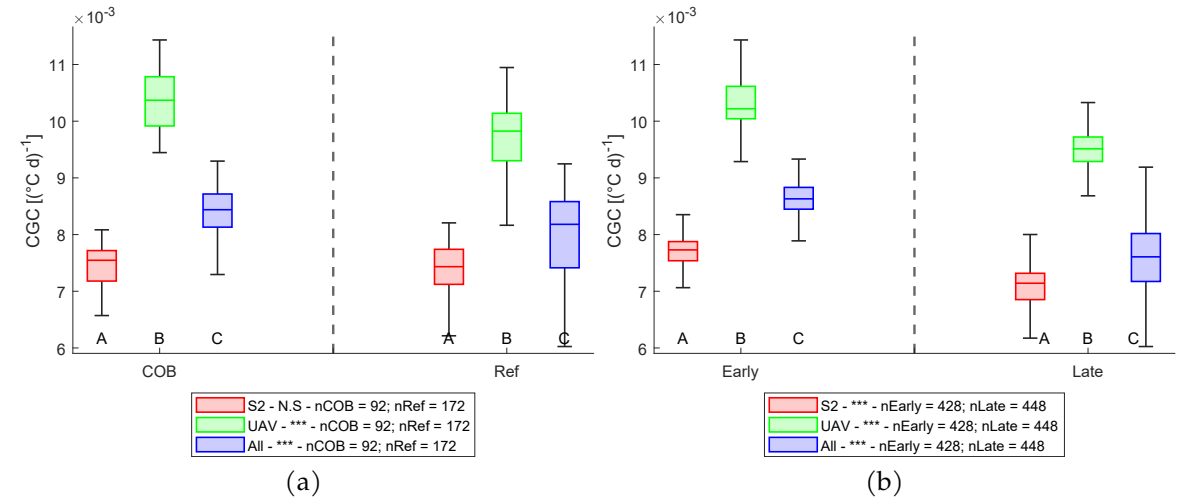

(a) (b)

Figure 4.11: CGC- 10 m - Maximal Slope - categorical covariate influences - a) Biochar Patches and b) Ploughing

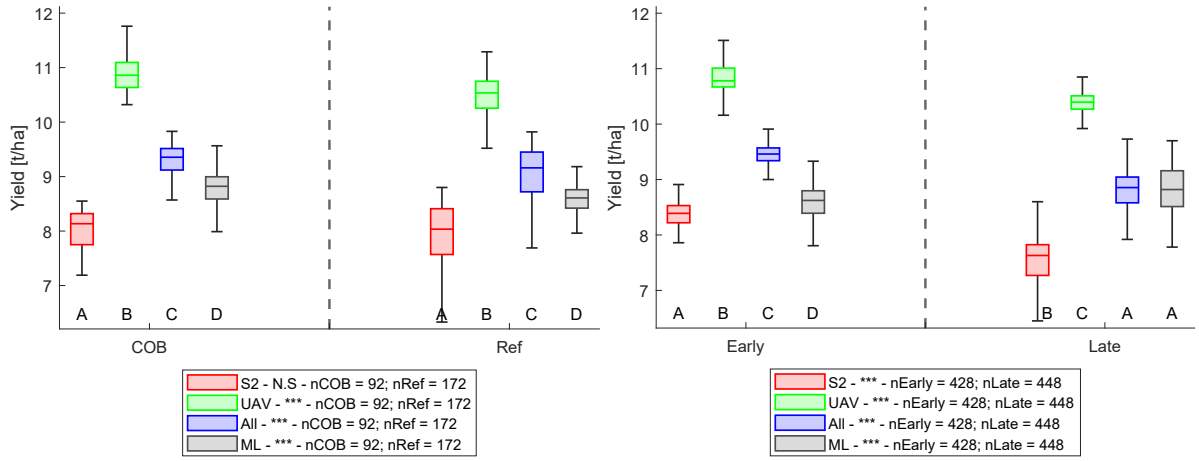

(a) (b)

Figure 4.12: Yield - categorical covariate influences - a) Biochar Patches and b) Ploughing

Influence of the topography

Many covariates describing topography have been tested to study their influence on crop growth parameters, but crop is indeed quite homogeneous in terms of topography, correlation between topographical indicators and crop growth parameters is really weak. Correlation plots are shown in Appendix A.7. SDevtN influence looks quite marginal on emergence date compared to ploughing, while SDevtN tends to have a positive effect on CGC and yield.

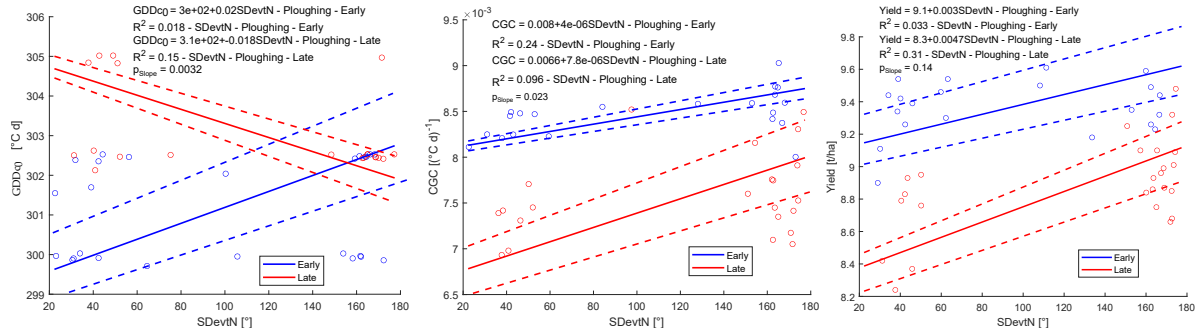

(a) (b) (c)

Figure 4.13: $GDDc_0$ - 10 m - Maximal Slope

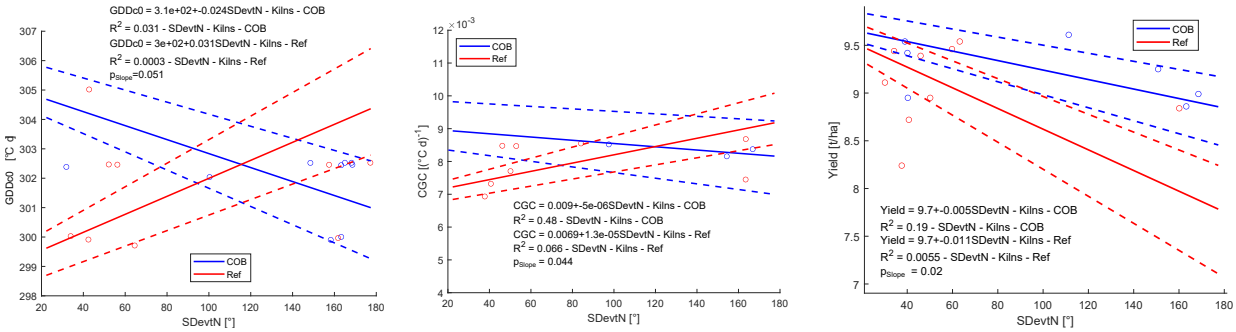

(a) (b) (c)

Figure 4.14: $GDDc_0$ - 10 m - Maximal Slope

Chapter 5

Conclusion, Limitations & Future Perspectives

This master thesis aimed to determine how suitable are UAV multispectral images to model crop growth compared to sentinel2 images. Addressing this question required developing tools to provide an exhaustive comparison of winter wheat growth models. The methodological outcome of this work consists of a growing curve parameter providing fitting a spatial description at a 10m resolution and using Aquacrop. In addition, a yield map is generated at this resolution, while remote sensing methods usually characterize crop growth processes at the scale of a complete parcel.

The results have shown that crop growth models exclusively based datasets on UAV are significantly different from crop growth curves solely relying on Sentinel2. Growth models estimated only from UAV methodology suggest an earlier, faster, and higher canopy expansion than those based on Sentinel2 images. Data combination provides intermediate results. Yield maps, which are correlated to the area under FCOVER growth curves, tend to confirm this trend; yields provided using UAV datasets are higher than those generated by Sentinel2 datasets. Data combination provides an intermediates estimation closer to a map based on a semiempirical model.

The spatial correlation between crop growth parameters estimated from the different maps is very low. This trend is also noticeable when analyzing crop growth models' relation with continuous covariables. Standard deviation to the North tends to be the topographic parameter having the more decisive influence on the growth process; besides the low correlation pattern, the southern slope tends to show earlier and steeper growth, while yields are also higher. Categorial variables trends are more visible; earlier plowed half of the field offers

higher growth rates and yields. Biochar area tends to start earlier, at a higher growth rate and slightly higher yields. (Heidarian Dehkordi et al. 2020) already noticed an earlier development while yields weren't significantly different between biochar patches and reference soil.

Future improvements could include building an alternative Aquacrop crop characterization dataset by calibrating coefficients directly from UAV images. This kind of calibration should be based on more complete experimental datasets to confront yield to ground truth to compare. A multisensor analysis based on UAV and combine harvester would produce accurate maps to submit yield characterization to a substantial robustness test (Stafford 2013; Morari et al. 2021). Using a parallel phenotyping platform to build a map of the canopy structure would provide additional high-resolution FCOVER maps as ground truths for FCOVER retrieval processes. Furthermore, alternative FCOVER computation, as described in (Sadeghi-Tehran et al. 2017; L. Li et al. 2018) based on the hypothesis of mixed pixel potentiality, could be investigated. Uncertainties estimations of this study rely on the quantification of FCOVER spatial heterogeneities; further researches could be led to describe experimental variability in FCOVER retrieval processes.

The use of remote sensing and UAV imagery to study crop growth processes is still a young research field, improvements in terms of UAV flight performances and image sensors There is no doubt that the scientific community's interest in these fields will continue to grow, given the expected advances in terms of flight performance and multispectral sensors.

Appendix A

Appendix

A.1 Yield approximation from

$$Y \propto \int_0^{\mathrm{GDDc}_{End}} \mathrm{FCOVER}\,\mathrm{d}\,\mathrm{GDDc} = \sum_i \int_{Start_i}^{End_i} \mathrm{FCOVER}\,\mathrm{d}\,\mathrm{GDDc}$$

$$(1.27) \longrightarrow \frac{0.5\,\mathrm{CC}_x - \mathrm{CC}_0}{\mathrm{CGC}}$$

$$(1.28) \longrightarrow \mathrm{CC}_x\left[\mathrm{GDDc}_{max} - \mathrm{GDDc}_{50\%}\right] + 0.25\frac{\mathrm{CC}_x}{\mathrm{CGC}}\left[1 - e^{-\,\mathrm{CGC}(\mathrm{GDDc}_{max} - \mathrm{GDDc}_{50\%})}\right]$$

$$(1.29) \longrightarrow \mathrm{CC}_x\left(\mathrm{GDDc}_{sen} - \mathrm{GDDc}_{max}\right)$$

$$(1.30) \longrightarrow \mathrm{CC}_x\left(\mathrm{GDDc}_{End} - \mathrm{GDDc}_{Sen}\right) - 0.05\,\mathrm{CC}_x\left(20\frac{\mathrm{CDC}}{\mathrm{CC}_x + 2.29}\cdots\right.$$

$$\left.\ldots - \left(\mathrm{GDDc}_{End} - \mathrm{GDDc}_{Sen}\right)\right)$$

$$\mathrm{CC}_x\frac{\mathrm{CC}_{x0} + 2.29}{3.33\,\mathrm{CDC}}\ln 21 - 0.05\,\mathrm{CC}_x\left(20\frac{\mathrm{CC}_{x0} + 2.29}{3.33\,\mathrm{CDC}} - \frac{\mathrm{CC}_{x0} + 2.29}{3.33\,\mathrm{CDC}}\ln 21\right)$$

$$\mathrm{CC}_x(0.95\ln 21 - 1)\frac{\mathrm{CC}_{x0} + 2.29}{3.33\,\mathrm{CDC}}$$

$$Y \propto \frac{0.5\,\mathrm{CC}_x - \mathrm{CC}_0}{\mathrm{CGC}} + CC_x\left[\mathrm{GDDc}_{max} - \mathrm{GDDc}_{50\%}\right] +$$
$$0.25\frac{\mathrm{CC}_x}{\mathrm{CGC}}\left[1 - e^{-\,\mathrm{CGC}(\mathrm{GDDc}_{max} - \mathrm{GDDc}_{50\%})}\right] +$$
$$\mathrm{CC}_x\left(\mathrm{GDDc}_{sen} - \mathrm{GDDc}_{max}\right) + \mathrm{CC}_x(0.95\ln 21 - 1)\frac{\mathrm{CC}_{x0} + 2.29}{3.33\,\mathrm{CDC}}$$

A.2 Phenology Model - UPVT

```
SENSIPHOT = 0;
PHOBASE = 6;          % Minimal day length to have a positive growth rate
PHOSAT = 20;          % Maximal day length - no additonal effect for long
```

```
RFPI = 1 - (1-SENSIPHOT)*(PHOSAT-TOD)/(PHOSAT-PHOBASE) ;
RFPI =  max(min(1,RFPI),0);
% Vernalisation
TFROID = 6.5; % Vernalization temperature
AMPFROID = 10;          % Amplitude of vernalization
JVC_MINI = 5;           % Minimal amount of cold for
JVI = min(max((1 - ((TFROID-TCULT)/AMPFROID).^2),0),1);          % Daily con
JVI(1:iStart) = 0;
JVC_V = 50;                                                      % Cumuluated vernal
RFVI = min(max((cumsum(JVI)-JVC_MINI)./((JVC_V-JVC_MINI)),0),1);
% Limitation in temperature
TDMIN = 0;     % Base temperature
TDMAX = 28;    % Maximal
TCXSTOP = 45;
UDEV((TCULT >= TDMIN) & (TCULT <= TDMAX)) = TCULT((TCULT >= TDMIN) & (TCU
UDEV((TCULT >= TDMAX) & (TCULT <= TCXSTOP)) =  (TCXSTOP-TCULT((TCULT >= TI
 UPVT = UDEV.*RFPI.*RFVI;
```

A.3 HYPRES Model

Table A.1: Complete system of equations describing *HYPRES* pedotransfer function - $\alpha^\star$, $n^\star$, $l^\star$ et $K_S^\star$ are transformed paramters of Mualem-van Genuchten model , θ_S saturation water content; C : clay fraction $(< 2\,\mu\mathrm{m})$; S : silt fraction $(2\,\mu\mathrm{m}$ et $50\,\mu\mathrm{m})$ OM cartbon content; D density $(\mathrm{g/cm^3})$; $\mathrm{topsoil}$ is one if horizon is topsoil and zero otherwise

$$
\begin{aligned}
\alpha^\star = {} & -14.96 + 0.03135 \cdot \mathrm{C} + 0.0351 \cdot \mathrm{S} + 0.646 \cdot \mathrm{OM} + 15.29 \cdot \mathrm{D} - 0.192 \cdot \mathrm{topsoil} \\
& - 4.671 \cdot \mathrm{D}^2 - 0.000781 \cdot \mathrm{C}^2 - 0.00687 \cdot \mathrm{OM}^2 + 0.0449 \cdot \mathrm{OM}^{-1} + 0.0663 \cdot \ln \mathrm{S} \\
& + 0.1482 \cdot \ln \mathrm{OM} - 0.04546 \cdot \mathrm{D\,S} - 0.4852 \cdot \mathrm{D} \cdot \mathrm{OM} + 0.00673 \cdot \mathrm{topsoil} \cdot \mathrm{C} \\
n^\star = {} & -25.23 - 0.02195 \cdot \mathrm{C} + 0.0074 \cdot \mathrm{S} - 0.1940 \cdot \mathrm{OM} + 45.5 \cdot \mathrm{D} - 7.24 \cdot \mathrm{D}^2 + 0.0003658 \cdot \mathrm{C}^2 \\
& + 0.002885 \cdot \mathrm{OM}^2 - 12.81 \cdot \mathrm{D}^{-1} - 0.1524 \cdot \mathrm{S}^{-1} - 0.01958 \cdot \mathrm{OM}^{-1} - 0.2876 \cdot \ln \mathrm{S} \\
& - 0.0709 \cdot \ln \mathrm{OM} - 44.6 \cdot \ln \mathrm{D} - 0.02264 \cdot \mathrm{D\,C} + 0.0896 \cdot \mathrm{D} \cdot \mathrm{OM} + 0.00718 \cdot \mathrm{topsoil} \cdot \mathrm{C} \\
l^\star = {} & 0.0202 + 0.0006193 \cdot \mathrm{C}^2 - 0.0011360 \cdot M^2 - 0.2316 \cdot \ln \mathrm{OM} - 0.03544 \cdot \mathrm{D} \cdot \mathrm{C} \\
& + 0.00283 \cdot \mathrm{D\,S} + 0.0488 \cdot \mathrm{D} \cdot \mathrm{OM} \\
K_S^\star = {} & 7.755 + 0.0352 \cdot \mathrm{S} + 0.93 \cdot \mathrm{topsoil} - 0.967 \cdot \mathrm{D}^2 - 0.000484 \cdot \mathrm{C}^2 - 0.000322 \cdot \mathrm{S}^2 \\
& + 0.001 \cdot \mathrm{S}^{-1} - 0.0748 \cdot \mathrm{OM}^{-1} - 0.643 \cdot \ln \mathrm{S} - 0.01398 \cdot \mathrm{D\,C} - 0.1673 \cdot \mathrm{D} \cdot \mathrm{OM} \\
& + 0.02986 \cdot \mathrm{topsoil} \cdot \mathrm{C} - 0.03305 \cdot \mathrm{topsoil} \cdot \mathrm{S} \\
\theta_S = {} & 0.7919 + 0.001691 \cdot \mathrm{C} - 0.29619 \cdot \mathrm{D} - 0.00001491 \cdot \mathrm{S}^2 + 0.0000821 \cdot \mathrm{OM}^2 + 0.02427 \cdot \mathrm{C}^{-1} \\
& + 0.01113 \cdot \mathrm{S}^{-1} + 0.01472 \cdot \ln \mathrm{S} - 0.00000733 \cdot \mathrm{OM} \cdot - 0.000619 \cdot \mathrm{D\,C} \\
& - 0.001183 \cdot \mathrm{D} \cdot \mathrm{OM} - 0.0001664 \cdot \mathrm{topsoil} \cdot \mathrm{S}
\end{aligned}
$$

A.4 Climate Datasets

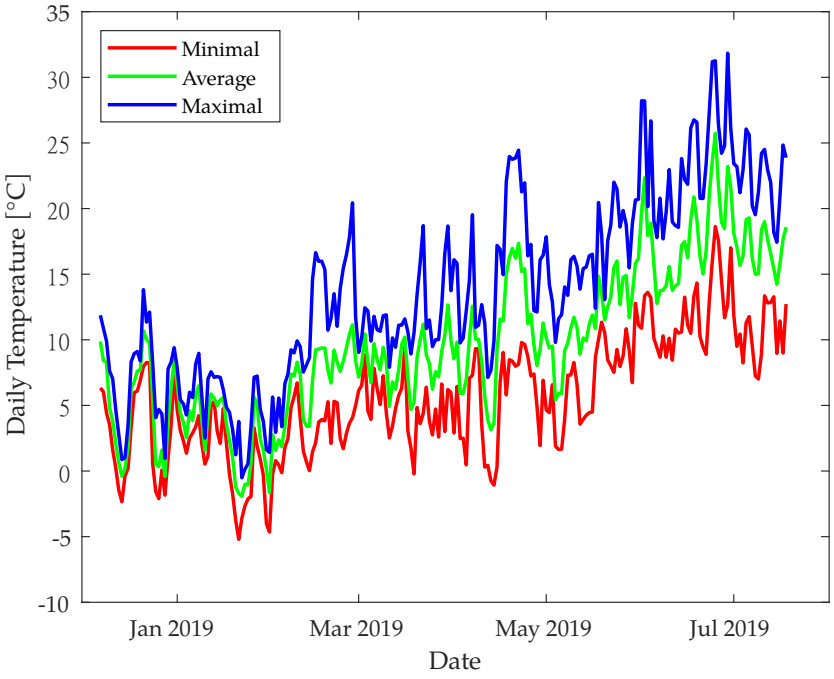
Minimal
Average
Maximal
Daily Temperature [°C]
35
30
25
20
15
10
5
0
-5
-10
Jan 2019
Mar 2019
May 2019
Jul 2019
Date

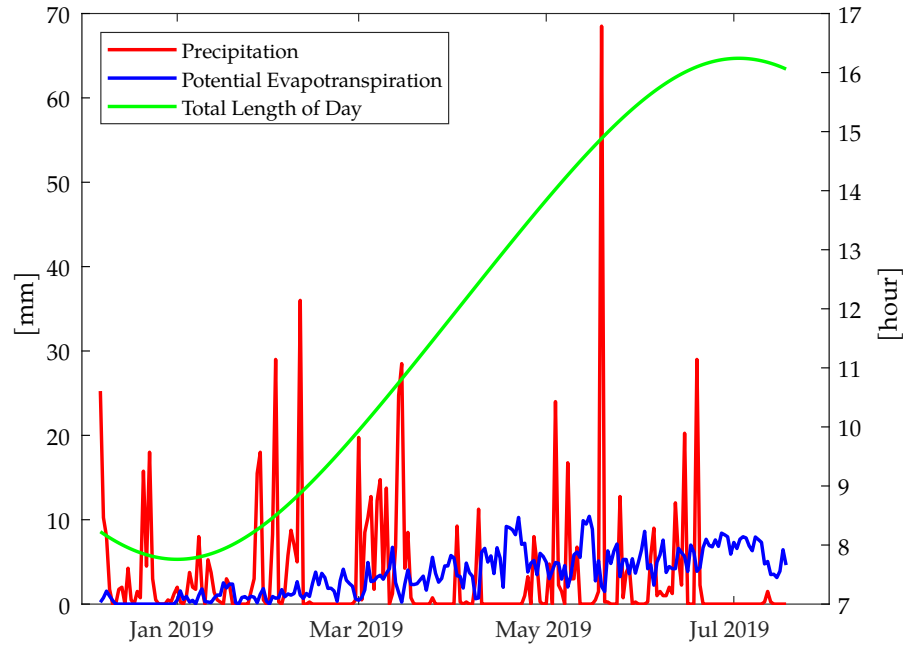
Precipitation
Potential Evapotranspiration
Total Length of Day
[mm]
70
60
50
40
30
20
10
0
[hour]
17
16
15
14
13
12
11
10
9
8
7
Jan 2019
Mar 2019
May 2019
Jul 2019

A.5 Ploughing Differential

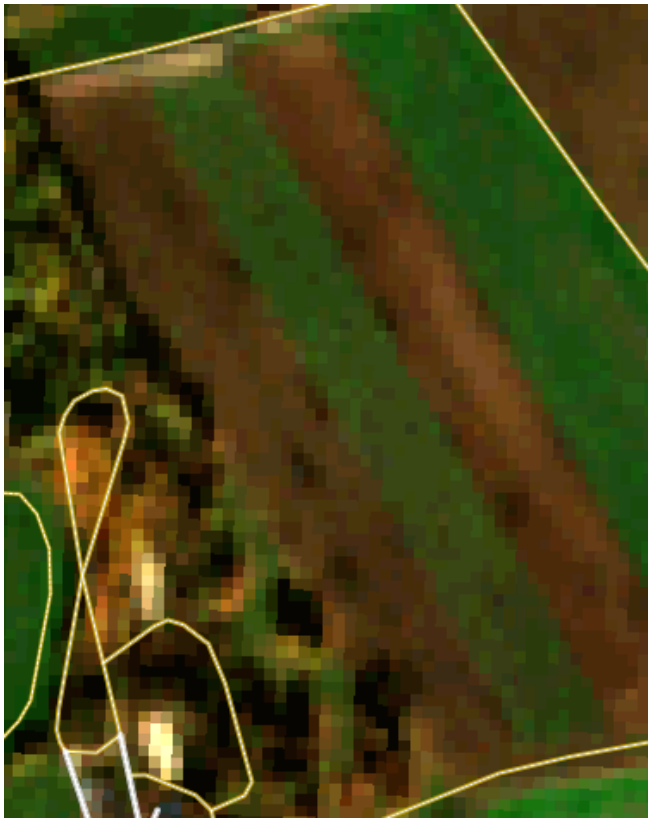

Figure 1.1: Sentinel2 - Situationt 18 november 2018

A.6 Additional Results - CC0 & CDC

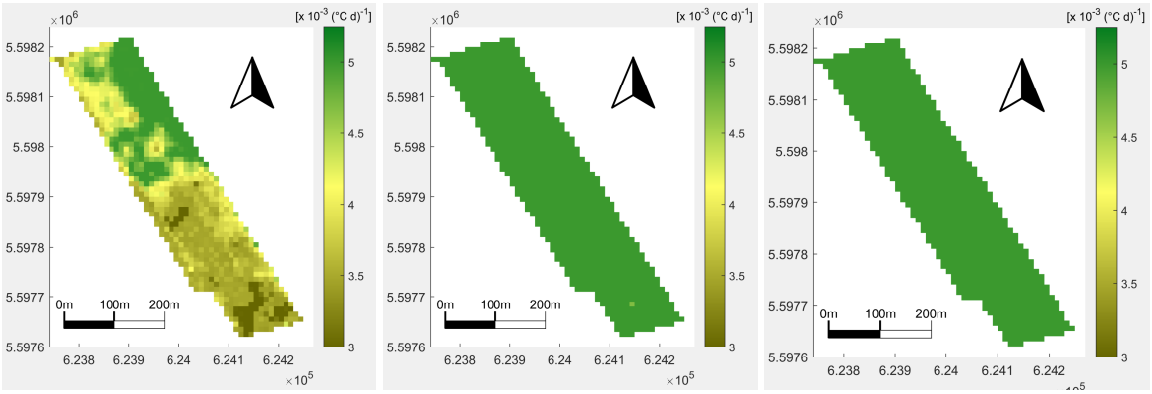

(a) (b) (c)

Figure 1.2: CDC - Canopy decline coefficient - 10 m - a) Sentinel2, b) UAV and c) S2+UAV

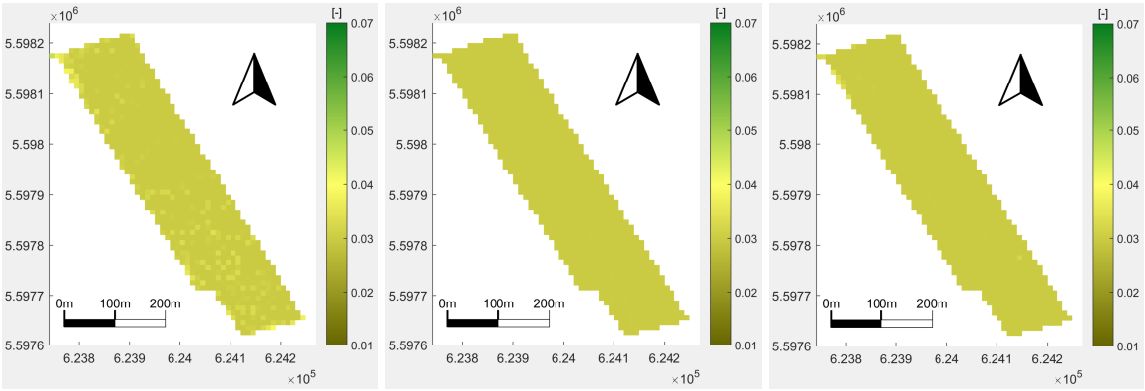

(a) (b) (c)

Figure 1.3: CC_0 - FCOVER at 90% of emergence - 10 m - a) Sentinel2, b) UAV and c) S2+UAV

A.7 Topography of the parcel

Local topography of the parcel -SRTM

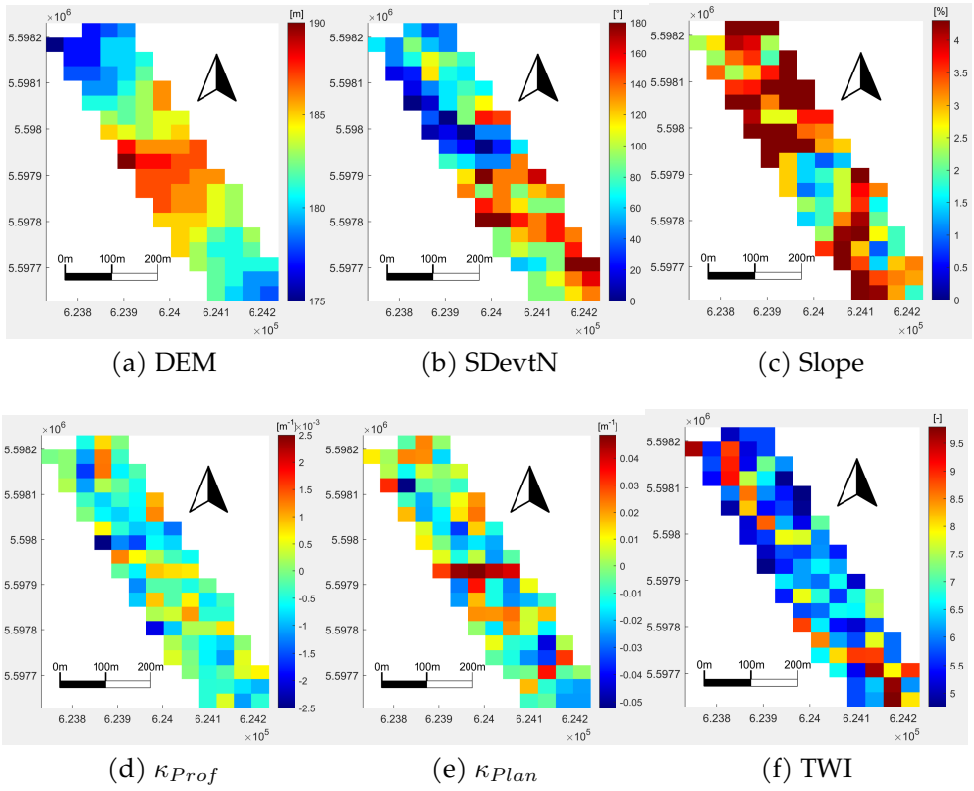

Figure 1.4: Topography - a) DEM, b) Slope, c) Deviation of slope towards North, d) Profile Curvature, e) Plan Curvature and f) Total Wetness Index

Influence of topography on model parameters

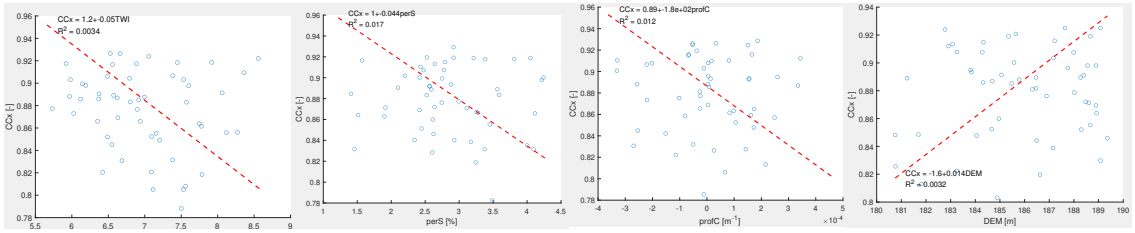

(a) CCx-TWI (b) CCx-Slope (c) CCx-κ_P (d) CCx- MNT

(e) CGC-TWI (f) CGC- Slope (g) CGC-κ_P (h) CGC- MNT

Figure 1.5: Sentinel2 vs Topography

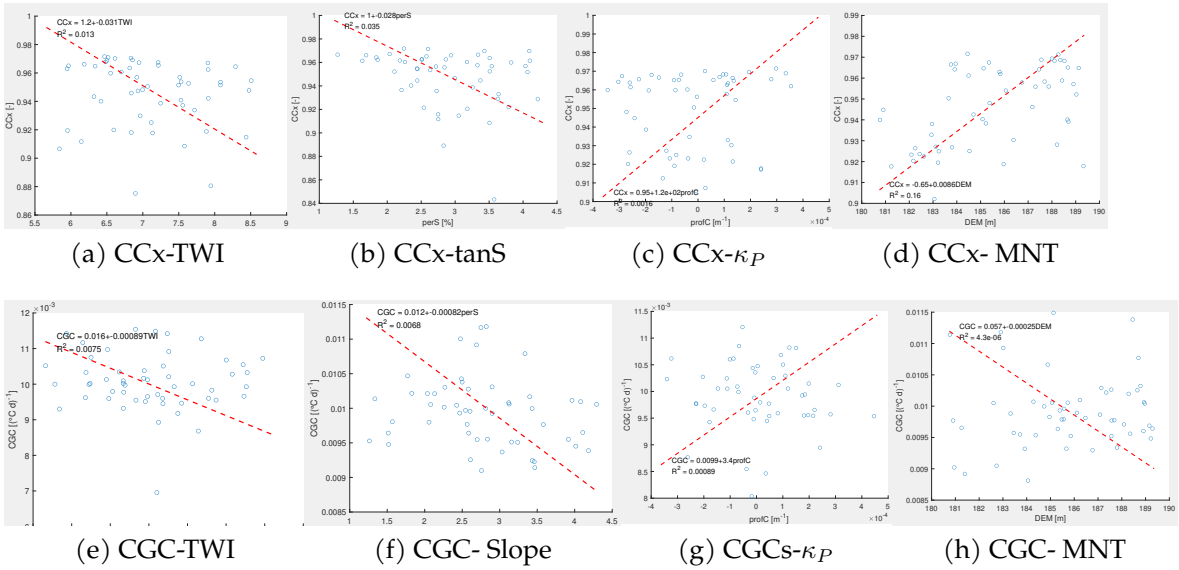

(a) CCx-TWI (b) CCx-tanS (c) CCx-κ_P (d) CCx- MNT

(e) CGC-TWI (f) CGC- Slope (g) CGCs-κ_P (h) CGC- MNT

Figure 1.6: UAV vs Topography

Bibliography

Fischer, Alberte (1994). "A model for the seasonal variations of vegetation indices in coarse resolution data and its inversion to extract crop parameters". In: *Remote Sensing of Environment* 48.2, pp. 220–230. ISSN: 00344257. DOI: 10.1016/0034-4257(94)90143-0.

Gate, Philippe. (1995). *Ecophysiologie du blé*. French. Paris: Tec & Doc Lavoisier.

Richter, O. and R. Seppelt (1996). "Quantitative aspects of sustainable agriculture". In: *Mathematics and Computers in Simulation* 42.2-3, pp. 263–269. ISSN: 03784754. DOI: 10.1016/0378-4754(95)00116-6.

Allen, R G et al. (1998). *Crop evapotranspiration. Guidelines for computing crop water requirements*. English.

Gutman, G. and A. Ignatov (Jan. 1998). "The derivation of the green vegetation fraction from NOAA/AVHRR data for use in numerical weather prediction models". In: *International Journal of Remote Sensing* 19.8, pp. 1533–1543. ISSN: 0143-1161. DOI: 10.1080/014311698215333. URL: https://www.tandfonline.com/doi/full/10.1080/014311698215333.

Carpenter, Alan T. et al. (1999). "Measuring and Monitoring Plant Populations". In: *Journal of Range Management* 52.5, p. 544. ISSN: 0022409X. DOI: 10.2307/4003786.

Wösten, J. H.M. et al. (1999). "Development and use of a database of hydraulic properties of European soils". In: *Geoderma* 90.3-4, pp. 169–185. ISSN: 00167061. DOI: 10.1016/S0016-7061(98)00132-3.

Abrahamsen, Per and Søren Hansen (2000). "Daisy: An open soil-crop-atmosphere system model". In: *Environmental Modelling and Software* 15.3, pp. 313–330. ISSN: 13648152. DOI: 10.1016/S1364-8152(00)00003-7.

"STICS: a generic model for simulating crops and their water and nitrogen balances. II. Model validation for wheat and maize" (Jan. 2002). In: *Agronomie* 22.1, pp. 69–92. ISSN: 0249-5627. DOI: 10.1051/agro:2001005. URL: http://www.edpsciences.org/10.1051/agro:2001005.

Berntsen, J. et al. (2003). "Evaluating nitrogen taxation scenarios using the dynamic whole farm simulation model FASSET". In: *Agricultural Systems* 76.3, pp. 817–839. ISSN: 0308521X. DOI: 10.1016/S0308-521X(02)00111-7.

"CropSyst, a cropping systems simulation model" (2003). In: *European Journal of Agronomy* 18.3-4, pp. 289–307. ISSN: 11610301. DOI: 10.1016/S1161-0301(02)00109-0.

Jones, J. W. et al. (2003). "The DSSAT cropping system model". In: 18.3-4, pp. 235–265. ISSN: 11610301. DOI: 10.1016/S1161-0301(02)00107-7.

Zhang, Xiaoyang et al. (2003). "Monitoring vegetation phenology using MODIS". In: *Remote Sensing of Environment* 84.3, pp. 471–475. ISSN: 00344257. DOI: 10.1016/S0034-4257(02)00135-9.

Badeck, Franz W. et al. (2004). "Responses of spring phenology to climate change". In: *New Phytologist* 162.2, pp. 295–309. ISSN: 0028646X. DOI: 10.1111/j.1469-8137.2004.01059.x.

Kersebaum, Kurt Christian (2007). "Modelling nitrogen dynamics in soil-crop systems with HERMES". In: *Nutrient Cycling in Agroecosystems* 77.1, pp. 39–52. ISSN: 13851314. DOI: 10.1007/s10705-006-9044-8.

Baret, Frédéric and Samuel Buis (2008). "Estimating Canopy Characteristics from Remote Sensing Observations: Review of Methods and Associated Problems". In: *Advances in Land Remote Sensing*. Dordrecht: Springer Netherlands, pp. 173–201. ISBN: 978-1-4020-6450-0. DOI: 10.1007/978-1-4020-6450-0_7. URL: https://doi.org/10.1007/978-1-4020-6450-0_7%20http://link.springer.com/10.1007/978-1-4020-6450-0_7.

Soudani, Kamel et al. (2008). "Evaluation of the onset of green-up in temperate deciduous broadleaf forests derived from Moderate Resolution Imaging Spectroradiometer (MODIS) data". In: *Remote Sensing of Environment* 112.5, pp. 2643–2655. ISSN: 00344257. DOI: 10.1016/j.rse.2007.12.004.

Doktor, Daniel et al. (2009). "Influence of heterogeneous landscapes on computed green-up dates based on daily AVHRR NDVI observations". In: *Remote Sensing of Environment* 113.12, pp. 2618–2632. ISSN: 00344257. DOI: 10.1016/j.rse.2009.07.020. URL: http://dx.doi.org/10.1016/j.rse.2009.07.020.

Sramkova, Z., E. Gregová, and E. Šturdík (2009). "Chemical composition and nutritional quality of wheat grain ". In: *Acta Chimica Slovaca* 2.1, pp. 115–138.

Brisson, Nadine et al. (2010). "Conceptual Basis, Formalisations and Parameterization of the Stics Crop Model". In: *Editons Quae*. URL: http://www.quae.com/en/r1291-conceptual-basis-formalisations-and-parameterization-of-the-stics-crop-model.html.

Wien, Jan Erik et al. (2010). *A web-based software system for model integration in impact assessments of agricultural and environmental policies*, pp. 207–234. ISBN: 9789048136186. DOI: 10.1007/978-90-4813618-6.

Bodson, B et al. (2011). "Implantation des cultures". In: *Livre Blanc Céréales - 2011*. Vol. 2242, pp. 1–11.

Doltra, Jordi, Mette Lægdsmand, and Jørgen E. Olesen (2011). "Cereal yield and quality as affected by nitrogen availability in organic and conventional arable crop rotations: A combined modeling and experimental approach". In: *European Journal of Agronomy* 34.2, pp. 83–95. ISSN: 11610301. DOI: 10.1016/j.eja.2010.11.002. URL: http://dx.doi.org/10.1016/j.eja.2010.11.002.

Legrain, Xavier et al. (2011). "Cartographie des sols en Belgique: Aperçu historique et présentation des travaux actuels de valorisation et de révision de la Carte Numérique des Sols de Wallonie". In: *Biotechnology, Agronomy and Society and Environment* 15.SPEC. ISSUE 2, pp. 647–656. ISSN: 13706233.

Palosuo, Taru et al. (2011). "Simulation of winter wheat yield and its variability in different climates of Europe: A comparison of eight crop growth models". In: *European Journal of Agronomy* 35.3, pp. 103–114. ISSN: 11610301. DOI: 10.1016/j.eja.2011.05.001.

Wise, Kiersten et al. (2011). "Managing Wheat by Growth Stage". In: *Purdue Extension* Feekes 2, pp. 3–8.

Cossani, C. Mariano and Matthew P. Reynolds (2012). "Physiological traits for improving heat tolerance in wheat". In: *Plant Physiology* 160.4, pp. 1710–1718. ISSN: 00320889. DOI: 10.1104/pp.112.207753.

Hoogenboom, Gerrit et al. (2012). *Improving Soil Fertility Recommendations in Africa using the Decision Support System for Agrotechnology Transfer (DSSAT)*. Ed. by Job Kihara et al. Dordrecht: Springer Netherlands, p. 283. ISBN: 978-94-007-2959-9. DOI: 10.1007/978-94-007-2960-5. URL: http://link.springer.com/10.1007/978-94-007-2960-5.

Boogaard, Hendrik et al. (2013). "A regional implementation of WOFOST for calculating yield gaps of autumn-sown wheat across the European Union". In: *Field Crops Research* 143, pp. 130–142. ISSN: 03784290. DOI: 10.1016/j.fcr.2012.11.005. URL: http://dx.doi.org/10.1016/j.fcr.2012.11.005.

Li, Genqiao et al. (2013). "Vernalization requirement duration in winter wheat is controlled by TaVRN-A1 at the protein level". In: *Plant Journal* 76.5, pp. 742–753. ISSN: 09607412. DOI: 10.1111/tpj.12326.

Stafford, John V (July 2013). *Precision agriculture '13*. Ed. by John V. Stafford. The Netherlands: Wageningen Academic Publishers. ISBN: 978-90-8686-224-5. DOI: 10.3920/978-90-8686-778-3. URL: https://www.wageningenacademic.com/doi/book/10.3920/978-90-8686-778-3.

Steduto, P. et al. (Apr. 2013). "Crop Yield Response to Water." In: *FAO Irrigation and Drainage* 49.2, pp. 311–311. ISSN: 0014-4797. DOI: 10.1017/S0014479712001366. URL: https://www.cambridge.org/core/article/crop-yield-response-to-water-fao-irrigation-

and-drainage-paper-66-by-p-steduto-t-c-hsiao-e-fereres-and-d-raes-rome-italy-food-and-agriculture-organization-of-the-united-nations-2012-pp-500-us10000-isbn-9789251072745-the-whole-report-can-be-downloaded-from-httpwwwfaoorgdocrep016i2800ei2800e00htm/6C90FC4E43F41042F8A5C9A510A281BE%20https://www.cambridge.org/core/product/identifier/S0014479712001366/type/journal_article.

Duan, Si Bo et al. (2014). "Inversion of the PROSAIL model to estimate leaf area index of maize, potato, and sunflower fields from unmanned aerial vehicle hyperspectral data". In: *International Journal of Applied Earth Observation and Geoinformation* 26.1, pp. 12–20. ISSN: 15698432. DOI: 10.1016/j.jag.2013.05.007. URL: http://dx.doi.org/10.1016/j.jag.2013.05.007.

Wellens, J. et al. (2014). *Manuel d'utilisation Aquacrop*. Tech. rep. Mai, p. 171. URL: www.ge-eau.org..

Bangare, Sunil L. et al. (2015). "Reviewing otsu's method for image thresholding". In: *International Journal of Applied Engineering Research* 10.9, pp. 21777–21783. ISSN: 09739769. DOI: 10.37622/ijaer/10.9.2015.21777-21783.

Fang, Fang (2015). "The Retrieval of Leaf Inclination Angle and Leaf Area Index in Maize". PhD thesis. Twente, p. 76.

Raschka, Sebastian (2015). *Python Machine Learning*. Packt Publishing - ebooks Account. ISBN: 1783555130.

Song, Wanjuan et al. (2015). "Extracting the green fractional vegetation cover from digital images using a shadow-resistant algorithm (SHAR-LABFVC)". In: *Remote Sensing* 7.8, pp. 10425–10443. ISSN: 20724292. DOI: 10.3390/rs70810425.

Merzougui, M et al. (2016). *Isodata et les algorithmes génétiques pour une classification non supervisée.* Tech. rep. May.

Vanuytrecht, Eline, Dirk Raes, and Patrick Willems (2016). "Regional and global climate projections increase mid-century yield variability and crop productivity in Belgium". In: *Regional Environmental Change* 16.3, pp. 659–672. ISSN: 1436378X. DOI: 10.1007/s10113-015-0773-6. URL: http://dx.doi.org/10.1007/s10113-015-0773-6.

Foster, T. et al. (Feb. 2017). "AquaCrop-OS: An open source version of FAO's crop water productivity model". In: *Agricultural Water Management* 181.November, pp. 18–22. ISSN: 03783774. DOI: 10.1016/j.agwat.2016.11.015. URL: https://linkinghub.elsevier.com/retrieve/pii/S0378377416304589.

Jay, Sylvain et al. (2017). "Retrieving LAI, chlorophyll and nitrogen contents in sugar beet crops from multi-angular optical remote sensing: Comparison of vegetation indices and PROSAIL inversion for field phenotyping". In: *Field Crops Research* 210.January, pp. 33–46.

ISSN: 03784290. DOI: 10.1016/j.fcr.2017.05.005. URL: http://dx.doi.org/10.1016/j.fcr.2017.05.005.

Sadeghi-Tehran, Pouria et al. (2017). "Multi-feature machine learning model for automatic segmentation of green fractional vegetation cover for high-throughput field phenotyping". In: *Plant Methods* 13.1, pp. 1–16. ISSN: 17464811. DOI: 10.1186/s13007-017-0253-8.

Berger, Katja et al. (2018). "Evaluation of the PROSAIL model capabilities for future hyperspectral model environments: A review study". In: *Remote Sensing* 10.1. ISSN: 20724292. DOI: 10.3390/rs10010085.

Eumetrain.org (2018). *Monitoring Vegetation From Space*. URL: http://www.eumetrain.org/data/3/36/contrib.htm.

Li, Linyuan et al. (2018). "A half-Gaussian fitting method for estimating fractional vegetation cover of corn crops using unmanned aerial vehicle images". In: *Agricultural and Forest Meteorology* 262.November, pp. 379–390. ISSN: 01681923. DOI: 10.1016/j.agrformet.2018.07.028.

Liu, Xiao-jun et al. (2018). "Leaf area index based nitrogen diagnosis in irrigated lowland rice". In: *Journal of Integrative Agriculture* 17.1, pp. 111–121. ISSN: 20953119. DOI: 10.1016/S2095-3119(17)61714-3. URL: http://dx.doi.org/10.1016/S2095-3119(17)61714-3.

Mougin, Eric et al. (2018). "A leaf area index, LAI, data set acquired in Sahelian rangelands (Gourma, Mali) over the 2005–2017 period". In: May. ISSN: 1866-3516. DOI: 10.5194/essd-2018-113.

Utstumo, Trygve et al. (2018). "Robotic in-row weed control in vegetables". In: *Computers and Electronics in Agriculture* 154.November, pp. 36–45. ISSN: 01681699. DOI: 10.1016/j.compag.2018.08.043.

Vanhamel, Thomas (2018). "Euroforecast - 2017-2018 drought in Belgium". In: *2017-2018 drought in Belgium*.

FAOSTAT (2019). *FAOSTAT statistical database*. URL: https://search.library.wisc.edu/catalog/999890171702121.

GDAL (2019). *GDAL - Sentinel-2 Products*. URL: https://gdal.org/drivers/raster/sentinel2.html.

IRM (2019). *Gembloux - Climate*. DOI: 19-06-21. URL: https://www.meteo.be/fr/gembloux.

Myers, Emily et al. (2019). "Assessing the impact of satellite revisit rate on estimation of corn phenological transition timing through shape model fitting". In: *Remote Sensing* 11.21, pp. 1–21. ISSN: 20724292. DOI: 10.3390/rs11212558.

Venske, Eduardo et al. (2019). "Bread wheat: a role model for plant domestication and breeding". In: *Hereditas* 156, p. 16. ISSN: 16015223. DOI: 10.1186/s41065-019-0093-9.

Weiss, Marie (2019). *LAI/fCover/fAPAR/Chlorophyll retrieval concepts and methods*. EO Open Science. URL: https://youtu.be/wHazjoVs5TU?t=562.

Gao, Lin et al. (2020). "Remote sensing algorithms for estimation of fractional vegetation cover using pure vegetation index values: A review". In: *ISPRS Journal of Photogrammetry and Remote Sensing* 159.November 2019, pp. 364–377. ISSN: 09242716. DOI: 10.1016/j.isprsjprs.2019.11.018. URL: https://doi.org/10.1016/j.isprsjprs.2019.11.018.

Heidarian Dehkordi, Ramin et al. (Aug. 2020). "Using UAV Collected RGB and Multispectral Images to Evaluate Winter Wheat Performance across a Site Characterized by Century-Old Biochar Patches in Belgium". In: *Remote Sensing* 12.15, p. 2504. ISSN: 2072-4292. DOI: 10.3390/rs12152504. URL: https://www.mdpi.com/2072-4292/12/15/2504.

Hyles, Jessica et al. (2020). "Phenology and related traits for wheat adaptation". In: *Heredity* 125.6, pp. 417–430. ISSN: 13652540. DOI: 10.1038/s41437-020-0320-1.

Liang, Shunlin and Jindi Wang (2020). *Fractional vegetation cover*, pp. 477–510. ISBN: 9780128158265. DOI: 10.1016/b978-0-12-815826-5.00012-x.

Rosillon, D. et al. (2020). "Deux nouveaux outils d'aide à la décision en céréales en Wallonie". In: *Livre Blanc "Céréales"* février, pp. 1–11.

Vavlas, Nikolaos Christos et al. (2020). "Deriving wheat crop productivity indicators using Sentinel-1 time series". In: *Remote Sensing* 12.15, pp. 1–22. ISSN: 20724292. DOI: 10.3390/RS12152385.

Weiss, Marie (2020). *S2ToolBox Level 2 products*. Tech. rep., p. 60. URL: https://step.esa.int/docs/extra/ATBD_S2ToolBox_L2B_V1.1.pdf.

Morari, F. et al. (2021). "Coupling proximal sensing, seasonal forecasts and crop modelling to optimize nitrogen variable rate application in durum wheat". In: *Precision Agriculture* 22.1, pp. 75–98. ISSN: 15731618. DOI: 10.1007/s11119-020-09730-6. URL: https://doi.org/10.1007/s11119-020-09730-6.

NASA (2021). *Digital Elevation Model - SRTM*. URL: https://www2.jpl.nasa.gov/srtm/.

USDA (2021). "Grain : World Markets and Trade". In: *United States Department of Agriculture Foreign Agricultural Service* May, pp. 1–11.

Wan, Liang et al. (2021). "A model for phenotyping crop fractional vegetation cover using imagery from unmanned aerial vehicles". In: *Journal of Experimental Botany* 72.13, pp. 4691–4707. ISSN: 14602431. DOI: 10.1093/jxb/erab194.